Robotics and Autonomous Systems 175 (2024) 104660

Contents lists available at ScienceDirect

Robotics and Autonomous Systems

journal homepage: www.elsevier.com/locate/robot

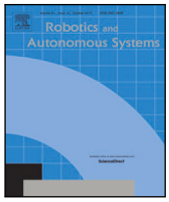

Lie-group modeling and simulation of a spherical robot, actuated by a yoke–pendulum system, rolling over a flat surface without slipping

Simone Fiori

Department of Information Engineering, Marches Polytechnic University, Via Brecce Bianche, Ancona, 60131, Italy

ARTICLE INFO

Keywords:
Lie-group theory
Non-holonomic Lagrange–d'Alembert principle
Non-conservative dynamical system
Non-holonomic dynamics
Spherical robot
Forward Euler method

ABSTRACT

The present paper aims at introducing a mathematical model of a spherical robot expressed in the language of Lie-group theory. Since the main component of motion is rotational, the space SO(3)3 of three-dimensional rotations plays a prominent role in its formulation. Because of friction to the ground, rotation of the external shell results in translational motion. Rolling without slipping implies a constraint on the tangential velocity of the robot at the contact point to the ground which makes it a non-holonomic dynamical system. The mathematical model is obtained upon writing a Lagrangian function that describes the mechanical system and by the Hamilton minimal-action principle modified through d'Alembert virtual work principle to account for non-conservative control actions as well as frictional reactions. The result of the modeling appears as a series of non-holonomic Euler–Poincaré equations of dynamics plus a series of auxiliary equations of reconstruction and advection type. A short discussion on the numerical simulation of such mathematical model complements the main analytic-mechanic development.

1. Introduction

Robots that are designed to operate in difficult terrains are specialized machines that are built to navigate and perform tasks in environments that are challenging for humans or traditional robots to access [1]. Such types of robots are often employed in search and rescue missions, construction and mining endeavors, agriculture, and scientific exploration [2]. Such machines might be equipped with a range of sensors and specialized hardware and software that enable them to sense and respond to their surroundings in order to navigate and perform tasks effectively. Some examples of robots that can operate in difficult terrains include tracked robots, legged robots and flying robots [3].

Spherical robots are complex mechanisms designed in the shape of a sphere [4–6]. They are typically self-contained, self-powered by an internal battery, and are able to move around by rolling on their spherical shell and to communicate over a wireless network. The concept of spherical robots, also known as 'ballbots,' dates back to the mid-20th century. The earliest ideas for these robots were primarily theoretical, with researchers envisioning a spherical shape as an efficient means of locomotion in certain environments. However, the technology to build practical spherical robots was limited at the time. In the 1980s and 1990s, researchers began to develop and experiment with the first functional spherical robots. Early prototypes were often large and unwieldy, but they demonstrated the potential of spherical designs.

The 2000s brought significant advances in miniaturization and control systems, enabling the development of smaller and more agile spherical robots. Researchers started to explore the potential applications of these robots in fields such as search and rescue, planetary exploration, and even entertainment. One of the pioneering examples was the *Sphero robot*, introduced as a consumer toy that could be controlled using a smartphone [7].

Spherical robots are deployed in a number of applications, including entertainment, education and scientific research [8]. One of the main advantages of spherical robots is their small size and ability to navigate through tight spaces and around obstacles. They are also relatively simple to manufacture and require fewer moving parts compared to other types of robots, which makes them potentially more reliable and easier to maintain. Locomotion in a spherical robot is attained through a number of internal actuators, such as a 'yoke' and a 'pendulum', that exploit the principle of momentum transfer to attain propulsion [9].

Spherical robots gained attention for their potential applications in planetary exploration. NASA, in particular, explored the concept of spherical robots for missions to celestial bodies like Mars [10]. As technology continued to advance, spherical robots found applications beyond planetary exploration and toys. Researchers and engineers began to explore their use in fields including agriculture (for autonomous farming) [11].

E-mail address: s.fiori@staff.univpm.it.
URL: http://web.dii.univpm.it/fiori.

https://doi.org/10.1016/j.robot.2024.104660
Received 9 November 2023; Received in revised form 4 January 2024; Accepted 8 February 2024
Available online 23 February 2024

The main advantages of a spherical design include low rolling resistance, omni-directional movement ability as well as amphibious capability [12]. In addition, a spherical robot can easily resume stability even after a physical collision. As a counterpart, due to their shape, spherical robots can be more challenging to control and balance compared to other types of robots, and they may not be suitable for tasks that require precise movements or manipulation [13].

Spherical robots often require mathematical models to describe their motion, dynamics, and control. Modeling a spherical robot is a challenging theoretical problem because of the structural complexity of their mechanical design, which entails strongly coupled dynamics among the shell, the yoke frame and the counter-weight pendulum [14]. The specific mathematical models may vary depending on the robot's design and purpose. Mathematical models for spherical robots have been developed according to a number of paradigms.

A first category of models fall in the realms of kinematic ones. In particular, models of direct kinematics relate the robot's control inputs (e.g., torques and forces) to its position and orientation in the environment and are essential for understanding how the robot moves in space. Inverse kinematics models are used to determine the control inputs necessary to achieve a desired position and orientation. For spherical robots, this can be complex due to their unique shape and mobility.

Mathematical models of spherical robots may be developed according to Newton–Euler equations, which describe the robot's motion dynamics, including the relationship between forces and accelerations. They are crucial for understanding how external forces affect the robot's motion. Alternatively, models may be developed according to Lagrangian dynamics, which provides a systematic way to derive equations of motion for complex mechanical systems, including spherical robots with multiple degrees of freedom.

A spherical robot rolling over a surface without slipping experiences friction with the ground and is hence a inherently non-holonomic system, since the non-slipping condition implies a precise form of constraint on the velocity of the contact point to the surface. In non-holonomic dynamics, a few drive inputs influence several degrees of freedom. Nonholonomic systems of the type sphere–sphere and sphere–plane have been extensively investigated in the past decades, being motivated by a number of engineering and physical applications in robotics, vibration absorption, railway engineering and in several others. For a comprehensive review, readers might consult [15–17].

Sensor fusion models for spherical robots equipped with sensing devices (e.g., cameras, Lidar, Inertial Measurement Units) combine data from multiple sensors to estimate the robot's state (e.g., position, orientation, and velocity) [18]. Quite interesting are so-termed 'terrain interaction models', which describe how a spherical robot interacts with different surfaces, considering factors like friction, rolling resistance, and contact forces [19,20]. Also, 'energy consumption models' estimate the energy consumption of a spherical robot based on its motion and control inputs [21,22]. They are crucial for designing efficient on-board power systems.

Proportional–Integral–Derivative (PID) control modeling produces mathematical models for PID controllers, which relate the error (difference between desired and actual states) to control signals (e.g., motor commands). Alternatively, Model Predictive Control (MPC) models include predictions of the robot's future states and are used in MPC-based control algorithms [23].

The choice of mathematical model depends on the specific design, sensors, and control algorithms employed by a spherical robot. Often simplifications and approximations are made to make convoluted mathematical models tractable for control and simulation. These models play a crucial role in designing, simulating, and controlling spherical robots for specific applications.

The present paper aims at presenting in details, and in a self-contained manner, two interlaced topics, namely:

Formulation of a model of a spherical robot: From a mechanical standpoint, a spherical robot may be regarded as a compound of rigid parts that are rotating one about another. The relative rotation of its constituents causes an overall rotation of the external shell of the robot. Friction to the ground, modeled as a non-holonomic constraint, then causes the translation of the robot with respect to a ground-fixed reference system. Since relative rotation of parts is the main component of motion, it appears appropriate to deploy a modeling technique based on the Lie group $SO(3)$ of 3D rotations, which will be recalled and applied in Section 2, where the Lagrangian function of the robot will be derived. In Section 3, the equations of motion will be sketched on the basis of the (non-holonomic) Lagrange–d'Alembert principle, which leads to the non-holonomic Euler–Poincaré equations for the studied robot. In Section 4, detailed calculations will be laid out in order to presents a complete set of equations of motion.

Numerical simulation: Given the specific formulation of the equations of motion based on Lie group theory, a specific Lie-group integration algorithm will be recalled and deployed to simulate numerically the behavior of the studied spherical robot in Section 5. A number of simple numerical simulations will be illustrated and commented, although more detailed numerical experiments, based on appropriate control design, is out of scope and will be presented in subsequent documents.

Section 6 will present some final remarks and will conclude this paper.

In summary, the present paper deals with a problem of a complicated nonholonomic dynamic system modeling using Lie-group background. Contact between a moving part and supporting surface is considered without a slipping possibility. The strategy of invoking a Lie-group representation shows effectiveness of this procedure providing possibility of compact and transparent formulation. A standing point of the present author is that Lie-group theory should be more abundantly used by researchers in works especially dealing with non-holonomic systems. The advantages of such approach would particularly stand out when working with non-holonomic bonds with higher time derivatives, e.g. controlled trajectories with prescribed parameters.

Ultimately, the aim of this paper is to represent a compact study devoted to the problem of modeling a complex robotic structure, which is worthy to be investigated at the field of the basic rational dynamics of nonholonomic systems. Results achieved in this paper open possibilities of applications not only in robotics, but also in other fields, such as space dynamics, wind and earthquake engineering, plasma physics, nano-technology, physiology, in some of which the present author has published contributions in the past.

2. Mathematical model of a spherical robot

In the present section, we shall recall some notation and relevant properties of Lie groups in Section 2.1. Section 2.2 presents a short review of inertia tensors for rigid objects in connection to Lie algebras. Section 2.3 outlines the mechanical configuration of the studied robot. Sections 2.4 to 2.6 present in a detailed fashion a derivation of the Lagrangian function associated to the studied robot as well as its reduced version. Section 2.7 presents a formulation of the non-holonomic constraint and yet a further instance of the Lagrangian function that incorporates such constraint. The reduced-constrained Lagrangian indeed constitutes the basis for the subsequent modeling endeavor.

2.1. Relevant notation and properties of Lie groups

It is instrumental to recall a few elements of notation from the theory of Lie groups:

- ***Matrix Lie group***: A smooth manifold $\mathbb{G}$ that is also an algebraic group is termed a Lie group. In this paper we focus on matrix Lie groups, namely on manifolds $\mathbb{G}$ endowed with matrix multiplication, matrix inversion and an identity matrix I as neutral element with respect to the matrix multiplication.
- ***Tangent bundle and its metrization***: Given a configuration $g \in \mathbb{G}$, the tangent space to $\mathbb{G}$ at g is denoted as $T_g\mathbb{G}$. The tangent bundle associated with a manifold-group $\mathbb{G}$ is denoted by $T\mathbb{G}$. The inner product of two tangent vectors $u, v \in T_g\mathbb{G}$ is denoted by $\langle u, v\rangle_g$.
- ***Lie algebra***: The tangent space $\mathfrak{g} := T_I\mathbb{G}$ to a Lie group at the identity is termed *Lie algebra*. Any Lie algebra is endowed with *Lie brackets*, denoted as $[\cdot,\cdot] : \mathfrak{g}\times\mathfrak{g} \to \mathfrak{g}$, and an *adjoint endomorphism* $\mathrm{ad}_\Omega\Psi := [\Omega, \Psi]$. On a matrix Lie algebra, it holds that $[\Omega, \Psi] := \Omega\Psi - \Psi\Omega$. Given a smooth function $\ell : \mathfrak{g} \to \mathbb{R}$, for a matrix Lie group one may define the *fiber derivative* of ℓ, $\frac{\partial \ell}{\partial \Omega} \in \mathfrak{g}$, at $\Omega \in \mathfrak{g}$ as the unique algebra element such that $\left\langle \frac{\partial \ell}{\partial \Omega}, \Psi \right\rangle_I = \mathrm{tr}\left((\mathrm{J}_\Omega \ell)^\top \Psi\right)$ for any $\Psi \in \mathfrak{g}$, where $\mathrm{J}_\Omega \ell$ denotes the Jacobian matrix of the function ℓ with respect to the matrix Ω and the symbol $^\top$ denotes matrix transpose.

The mathematical model of a spherical robot is based on a couple manifolds, namely:

- ***Rotation group and algebra***: The matrix Lie group of 3-dimensional rotations defined as $\mathrm{SO}(3) := \{R \in \mathbb{R}^{3\times 3} \mid R^\top R = RR^\top = I_3,\ \det(R) = +1\}$. Its Lie algebra is $\mathfrak{so}(3) := \{\Omega \in \mathbb{R}^{3\times 3} \mid \Omega + \Omega^\top = 0\}$. The symbol I_3 represents a 3×3 identity matrix. It is straightforward to see that any matrix $\Omega \in \mathfrak{so}(3)$ is skew symmetric and that the matrix $-\Omega^2$ is non-negative definite. The matrix commutator in $\mathfrak{so}(3)$ is a skew-symmetric bilinear form, namely $[\Omega, \Psi] + [\Psi, \Omega] = 0$ for any $\Omega, \Psi \in \mathfrak{so}(3)$.
- ***Two-sphere and tangent bundle***: The two-dimensional sphere $\mathrm{S}^2 := \{\eta \in \mathbb{R}^3 \mid \eta^\top\eta = 1\}$, whose tangent space at a point η is $T_\eta\mathrm{S}^2 = \{\beta \in \mathbb{R}^3 \mid \eta^\top\beta = 0\}$.

For more details on manifolds, Lie groups, coordinate-free representations in system theory and control, interested readers might consult the tutorial paper [24].

It is convenient to recall that, in $\mathbb{R}^3$, it is defined a cross product denoted as $\times$ which, given two vectors $x, z \in \mathbb{R}^3$, returns a vector $x \times z$ orthogonal to the plane spanned by its arguments. A frequently-invoked relationship to compute the norm of a cross-product is

$$\|x \times z\|^2 = \|x\|^2\|z\|^2 - (x^\top z)^2. \tag{1}$$

It is also instrumental to define the operator $[\![\cdot]\!] : \mathbb{R}^3 \to \mathfrak{so}(3)$ as:

$$[\![x]\!] := \begin{bmatrix} 0 & -x_3 & x_2 \\ x_3 & 0 & -x_1 \\ -x_2 & x_1 & 0 \end{bmatrix}. \tag{2}$$

There exists a noticeable interplay between the operators $\times$ and $[\![\cdot]\!]$, in fact, it is straightforward to show that $x \times z = [\![x]\!]z$ (as long as x and z are represented as column vectors).

Since any skew-symmetric matrix in $\mathfrak{so}(3)$ may be written as in the right-hand side of (2), it is convenient to define a basis of this vector space as $\mathfrak{so}(3) = \mathrm{span}(\Sigma_Y, \Sigma_P, \Sigma_C)$, with

$$\Sigma_Y := \begin{bmatrix} 0 & 0 & 0 \\ 0 & 0 & -1 \\ 0 & 1 & 0 \end{bmatrix},\ \Sigma_P := \begin{bmatrix} 0 & 0 & 1 \\ 0 & 0 & 0 \\ -1 & 0 & 0 \end{bmatrix},\ \Sigma_C := \begin{bmatrix} 0 & -1 & 0 \\ 1 & 0 & 0 \\ 0 & 0 & 0 \end{bmatrix}. \tag{3}$$

The canonical product in the linear space $\mathfrak{so}(3)$ is denoted as $\langle \Omega, \Psi\rangle^{\mathfrak{so}(3)} := \mathrm{tr}(\Omega^\top\Psi) = -\mathrm{tr}(\Omega\Psi)$ for any $\Omega, \Psi \in \mathfrak{so}(3)$.

An operator that arises naturally in the equations is the *adjoint representation*, denoted as $\mathrm{Ad} : \mathrm{SO}(3)\times\mathfrak{so}(3) \to \mathfrak{so}(3)$ and defined as

$$\mathrm{Ad}_R(\Omega) := R\Omega R^\top. \tag{4}$$

Both the adjoint endomorphism and the adjoint representation operator stem from the 'inner isomorphism' of a Lie group as recalled, e.g., in [24].

Moreover, it is convenient to recall a property of the matrix 'trace' operator, namely $\mathrm{tr}(ABC) = \mathrm{tr}(BCA) = \mathrm{tr}(CAB)$ for any compatible matrices A, B, C. From this property it follows that, for every vector $x \in \mathbb{R}^3$, it holds that

$$\|x\|^2 = \mathrm{tr}(xx^\top). \tag{5}$$

2.2. Brief review of inertia tensors: definitions and properties

The aim of the present section is to review the notion of inertia tensor (or inertia matrix) from rational mechanics in connection with the kinetic energy of a rigid body. In particular, we shall recall the notion of *standard* inertia tensor, *non-standard* inertia tensor, and Huygens–Steiner theorem expressed in matrix Lie-algebra form.

Let us consider a continuous rigid body $\mathscr{B}$ and let us introduce a body-fixed reference system $\mathcal{F}_\mathscr{B}$ whose center coincides to the center of mass of the body. Let us now consider an infinitesimal volume element, whose position in $\mathcal{F}_\mathscr{B}$ is described by the vector $q \in \mathbb{R}^3$ and whose mass is denoted by $\mathrm{d}m$. We shall assume that the body is rotating with an angular velocity $\omega \in \mathbb{R}^3$, which describes its rotation speed as well as the orientation of its instantaneous rotation axis.

The (rotational) kinetic energy of the body is defined through the volume integral

$$K := \frac{1}{2}\int_\mathscr{B} \|\omega \times q\|^2 \mathrm{d}m. \tag{6}$$

By the property (1), the above integral may be rewritten as

$$K = \frac{1}{2}\int_{\mathscr{B}} (\|\omega\|^2\|q\|^2 - (\omega^\top q)^2)\mathrm{d}m = \frac{1}{2}\omega^\top J\omega \tag{7}$$

where we have defined the 3×3 matrix

$$J := \int_{\mathscr{B}} ((q^\top q)I_3 - qq^\top)\mathrm{d}m, \tag{8}$$

that is referred to as *standard inertia tensor*. By splitting the position vector q into Cartesian components and by making the calculations explicit, the standard expression of the matrix J available in textbooks is recovered. We shall not make such expression explicit and we shall merely observe that the expressions of J for most standard three-dimensional and two-dimensional shapes are available in physics and rational mechanics textbooks.

Let us now introduce an inertial reference system $\mathcal{F}_\mathrm{E}$. The kinetic energy of a rigid body may be expressed in a different way by introducing the matrix $R \in \mathrm{SO}(3)$ that rotates the body-fixed reference system and takes it to coincide to the inertial reference system. In this framework, the velocity of a volume element reads $\dot{R}q$, hence the kinetic energy of the rigid body, by virtue of the property (5), takes the expression

$$K = \frac{1}{2}\int_{\mathscr{B}} \mathrm{tr}((\dot{R}q)(\dot{R}q)^\top)\mathrm{d}m. \tag{9}$$

By recalling that $\dot{R} = R\Omega$, with $\Omega \in \mathfrak{so}(3)$ denoting the angular velocity matrix of the rigid body expressed in the Lie-algebra framework, it turns out that

$$K = \frac{1}{2}\mathrm{tr}(\Omega\hat{J}\Omega^\top), \tag{10}$$

where we have introduced the matrix

$$\hat{J} = \int_{\mathscr{B}} qq^\top \mathrm{d}m \tag{11}$$

which is referred to as *non-standard inertia tensor*.

The tensors J and $\hat{J}$ are closely related. In fact, from the definition (8), it turns out that

$$J = I_3\mathrm{tr}\left(\int_{\mathscr{B}} qq^\top \mathrm{d}m\right) - \int_{\mathscr{B}} qq^\top \mathrm{d}m = \mathrm{tr}(\hat{J})I_3 - \hat{J}. \tag{12}$$

The inverse relationship is more convenient. Let us notice from the above that $\mathrm{tr}(J) = 3\mathrm{tr}(\hat{J}) - \mathrm{tr}(\hat{J})$, hence $\mathrm{tr}(\hat{J}) = \frac{1}{2}\mathrm{tr}(J)$, therefore

$$\hat{J} = \tfrac{1}{2}\mathrm{tr}(J)I_3 - J. \tag{13}$$

The non-standard inertia tensor may be hence calculated easily whenever the standard one is known for a given object.

Let us recall a further expression of the standard inertia tensor that allows expressing the classical Huygens–Steiner formula in a compact way. The kinetic energy (6) may be recast as

$$K = \frac{1}{2}\int_{\mathscr{B}} \|q \times \omega\|^2 \mathrm{d}m = \frac{1}{2}\int_{\mathscr{B}} \|[\![q]\!]\omega\|^2 \mathrm{d}m = \frac{1}{2}\int_{\mathscr{B}} \omega^\top [\![q]\!]^\top [\![q]\!]\omega \,\mathrm{d}m, \tag{14}$$

which coincides with the expression (7) where the inertia tensor takes the expression

$$J = -\int_{\mathscr{B}} [\![q]\!]^2 \mathrm{d}m, \tag{15}$$

which is equivalent to the expression (8).

Now, the matrix J represents the inertia tensor of a rigid body with respect to its center of mass. Let us denote by J_L the inertia tensor with respect to a point whose position, in the reference system $\mathcal{F}_{\mathscr{B}}$, is denoted as $p \in \mathbb{R}^3$. It holds that

$$J_L = -\int_{\mathscr{B}} [\![q+p]\!]^2 \mathrm{d}m = -\int_{\mathscr{B}} ([\![q]\!] + [\![p]\!])^2 \mathrm{d}m = -\int_{\mathscr{B}} ([\![q]\!]^2 + [\![q]\!][\![p]\!] + [\![p]\!][\![q]\!] + [\![p]\!]^2)\mathrm{d}m. \tag{16}$$

The first integral coincides with J, while the second and third integral are null because $\int_{\mathscr{B}} [\![q]\!]\mathrm{d}m = [\![\int_{\mathscr{B}} q\,\mathrm{d}m]\!] = 0$ by definition of center of mass. In conclusion, it holds that

$$J_L = J - [\![p]\!]^2 m_{\mathscr{B}}, \tag{17}$$

where $m_{\mathscr{B}} := \int_{\mathscr{B}} \mathrm{d}m$ denotes the total mass of the body. The obtained expression represents the Huygens–Steiner formula written in matrix (Lie-algebra) notation, which enables one to express the inertia tensor of an object that is in a state of rotation around an off-central axis.

2.3. Mechanical configuration of the spherical robot

In the present section, we shall revise the mechanical structure of the spherical robot described in [25,26], therein referred to as 'BYQ-III' model design. The locomotion mechanism of such robot consists of two separate actuators: a *steer motor*, which mainly controls the direction of motion of the robot by tilting a counter-weight pendulum, and a *drive motor*, which causes forward and/or backward acceleration by swinging the counter-weight pendulum indirectly through a *yoke*.

An inertial reference system $\mathcal{F}_\mathrm{E}$ serves as a basis to describe the attitude of the robot as well as to develop its mathematical model. A schematic of the studied spherical robot is displayed in Fig. 1.

The mechanical structure of the studied spherical robot is described succinctly as follows:

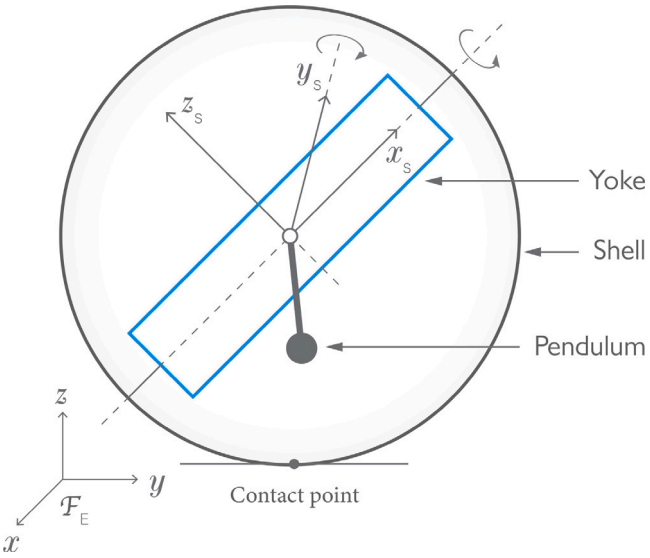

Fig. 1. A schematic of a yoke–pendulum actuated spherical robot. The frame on the left-bottom corner represents the inertial reference system $\mathcal{F}_E$. The axes labeled x_s, y_s and z_s denote the shell-fixed reference system $\mathcal{F}_S$. The semi-circular arrows mark the rotation axes of the yoke and pendulum.

- ***Spherical hull***: The exterior of the spherical robot is made of a thin spherical shell $\mathscr{S}$. A reference system $\mathcal{F}_S$ is attached to the shell. The orientation of the robot with respect to the inertial frame is described by a rotation matrix $R_S \in \mathrm{SO}(3)$: the matrix R_S takes the Cartesian axes of the reference system $\mathcal{F}_S$ to coincide to the Cartesian axes of the reference system $\mathcal{F}_E$. A thin spherical shell of mass m_S and radius r is characterized by an inertia tensor of the type $J_S := j_S I_3$, where $j_S := \frac{2}{3} m_S r^2$. The center of mass of the spherical hull coincides with its geometric center. For a thin spherical shell, it holds that $\hat{J}_S = \frac{1}{2}\mathrm{tr}(J_S) I_3 - J_S = \frac{1}{2} j_S I_3$.
- ***Internal yoke***: The spherical robot contains a yoke $\mathscr{Y}$ (sometimes also referred to as gimbal). A reference system $\mathcal{F}_Y$ is attached to the yoke. The yoke has a fixed axis, say the x axis, about which it spins and we assume that the x axis of the reference system $\mathcal{F}_Y$ coincides with the x axis of the spherical shell's reference system $\mathcal{F}_S$. The orientation of the yoke with respect to the shell is described by a rotation matrix $R_Y \in \mathrm{SO}(3)$. The center of mass of the yoke coincides always with the center of mass of the sphere and its mass is denoted as m_Y. The yoke is assumed to take the shape of a thin rectangular frame laying on the x-y plane of the yoke-fixed reference. The frame is supposed to be made of four thin rods, two of length b and mass m_b, and two of length h and mass m_h. By using the tabulated value of the inertia tensor of a thin rod and the Huygens–Steiner formula, we got an expression for the standard inertia tensor J_Y of the form $\begin{bmatrix} j_{xx} & 0 & 0 \\ 0 & j_{yy} & 0 \\ 0 & 0 & j_{xx}+j_{yy} \end{bmatrix}$, where $j_{xx} := (\frac{m_b}{6} + \frac{m_h}{2})b^2$ and $j_{yy} := (\frac{m_b}{2} + \frac{m_h}{6})h^2$. The non-standard inertia tensor $\hat{J}_Y$ hence takes the diagonal form $\begin{bmatrix} j_{yy} & 0 & 0 \\ 0 & j_{xx} & 0 \\ 0 & 0 & 0 \end{bmatrix}$. The total mass of the yoke takes value $m_Y = 2(m_b + m_h)$.
- ***Counter-weight pendulum***: The spherical robot contains a pendulum $\mathscr{P}$, which is made by a slender rod of length l attached by one end to the center of mass of the yoke/sphere. Let us attach a reference system $\mathcal{F}_P$ to the pendulum. The pendulum lies along the $-z$ axis of its own reference system and swings around its y axis, which coincides always with the y axis of the yoke. The orientation of the pendulum with respect to the yoke is described by a rotation matrix $R_P \in \mathrm{SO}(3)$. The mass of the pendulum is denoted by m_P. Assuming such mass to be uniformly distributed along the rod, its inertia tensor is $J_P := \begin{bmatrix} j_P & 0 & 0 \\ 0 & j_P & 0 \\ 0 & 0 & 0 \end{bmatrix}$ with $j_P := \frac{1}{3} m_P l^2$. Its non-standard inertia tensor hence reads $\hat{J}_P = \frac{1}{2}\mathrm{tr}(J_P) I_3 - J_P = \begin{bmatrix} 0 & 0 & 0 \\ 0 & 0 & 0 \\ 0 & 0 & j_P \end{bmatrix}$.
- The coordinate of the center of the spherical robot with respect to the inertial reference system is denoted as $q \in \mathbb{R}^2 \times \{r\}$.
- The center of mass $\bar{c}_P$ of the pendulum coincides with the geometric center of the pendulum whose coordinate, in the reference system $\mathcal{F}_P$, is $-\frac{l}{2} e_z$, where $e_z := [0\ 0\ 1]^\top$.

The configuration of the spherical robot at a given time is described by the quadruple (R_S, R_Y, R_P, q), hence the configuration manifold for this vehicle is $\mathbb{Q} := \mathrm{SO}(3) \times \mathrm{SO}(3) \times \mathrm{SO}(3) \times (\mathbb{R}^2 \times \{r\})$. The tangent space at a given state is

$$\begin{aligned} T_{(R_S,R_Y,R_P,q)}\mathbb{Q} &= T_{R_S}\mathrm{SO}(3) \times T_{R_Y}\mathrm{SO}(3) \times T_{R_P}\mathrm{SO}(3) \times (\mathbb{R}^2 \times \{0\}) \\ &= (R_S \mathfrak{so}(3)) \times (R_Y \mathfrak{so}(3)) \times (R_P \mathfrak{so}(3)) \times (\mathbb{R}^2 \times \{0\}), \end{aligned} \tag{18}$$

where a matrix times a Lie algebra denotes a multiplication of the matrix by each element of the algebra.

2.4. Kinetic energy of the shell, yoke and pendulum

Let us denote by q_S the coordinate of an infinitesimal volume of mass $\mathrm{d}m$ belonging to the spherical shell in the coordinate system $\mathcal{F}_S$. The coordinate of such volume in the inertial reference system is given by $q + R_S q_S$, hence the kinetic energy of the shell in the inertial system is given by the volume integral

$$K_S := \frac{1}{2}\int_{\mathscr{S}} \left\| \frac{\mathrm{d}}{\mathrm{d}t}(q + R_S q_S) \right\|^2 \mathrm{d}m = \frac{1}{2}\int_{\mathscr{S}} \|\dot{q}\|^2 \mathrm{d}m + \frac{1}{2}\int_{\mathscr{S}} \|\dot{R}_S q_S\|^2 \mathrm{d}m + \int_{\mathscr{S}} \dot{q}^\top \dot{R}_S q_S \,\mathrm{d}m. \tag{19}$$

Recalling the property (5) and introducing the angular velocity matrix $\Omega_S := R_S^\top \dot{R}_S \in \mathfrak{so}(3)$, we get:

$$\begin{aligned} K_S &= \frac{1}{2} m_S \|\dot{q}\|^2 + \frac{1}{2}\int_{\mathscr{S}} \mathrm{tr}(R_s \Omega_S q_S q_S^\top \Omega_S^\top R_S^\top)\mathrm{d}m + \dot{q}^\top \dot{R}_S \int_{\mathscr{S}} q_S \,\mathrm{d}m, \\ &= \frac{1}{2} m_S \|\dot{q}\|^2 + \frac{1}{2}\mathrm{tr}(\cancel{R_S}\, \Omega_S \hat{J}_S \Omega_S^\top \cancel{R_S^\top}) + m_S \dot{q}^\top \dot{R}_S \bar{c}_S, \end{aligned} \tag{20}$$

where we have used the cyclic commutation property of the matrix trace to cross out the instances of R_S from the second integral and

$$m_S := \int_{\mathscr{S}} \mathrm{d}m, \;\; \hat{J}_S := \int_{\mathscr{S}} q_S q_S^\top \mathrm{d}m, \;\; \bar{c}_S := \frac{1}{m_S}\int_{\mathscr{S}} q_S \,\mathrm{d}m. \tag{21}$$

The quantity $\bar{c}_S \in \mathbb{R}^3$ represents the coordinate of the center of mass of the shell in the reference system $\mathcal{F}_S$ which, by hypothesis, coincides with its geometric center, therefore $\bar{c}_S = 0$. In conclusion

$$K_S = \frac{1}{2} m_S \|\dot{q}\|^2 + \frac{1}{2}\mathrm{tr}(\Omega_S \hat{J}_S \Omega_S^\top).$$

As a result, the kinetic energy of the shell appears as the sum of a term that quantifies the translational kinetic energy of its center and of a term that quantifies the rotational kinetic energy of the shell. It is worth remarking that the variable Ω_S represents the rolling speed of the robot as seen from the rolling reference system $\mathcal{F}_S$.

Let us denote by q_Y the coordinate of an infinitesimal volume of mass $\mathrm{d}m$ belonging to the yoke frame in the coordinate system $\mathcal{F}_Y$. The coordinate of such volume in the inertial reference system is given by $q + R_S R_Y q_Y$, hence the kinetic energy of the yoke in the inertial reference system is given by

$$K_Y := \frac{1}{2}\int_{\mathscr{Y}} \left\| \frac{\mathrm{d}}{\mathrm{d}t}(q + R_S R_Y q_Y) \right\|^2 \mathrm{d}m = \frac{1}{2}\int_{\mathscr{Y}} \|\dot{q} + \dot{R}_s R_Y q_Y + R_S \dot{R}_Y q_Y\|^2 \mathrm{d}m. \tag{22}$$

Going through similar calculations as before, we get

$$\begin{aligned} K_Y = {} & \frac{1}{2} m_Y \|\dot{q}\|^2 + \frac{1}{2}\mathrm{tr}(\dot{R}_S R_Y \hat{J}_Y R_Y^\top \dot{R}_S^\top) + \frac{1}{2}\mathrm{tr}(R_S \dot{R}_Y \hat{J}_Y \dot{R}_Y^\top R_S^\top) \\ & + m_Y \dot{q}^\top \dot{R}_S R_Y \bar{c}_Y + m_Y \dot{q}^\top R_S \dot{R}_Y \bar{c}_Y + \mathrm{tr}(\dot{R}_S R_Y \hat{J}_Y \dot{R}_Y^\top R_S^\top), \end{aligned} \tag{23}$$

where

$$m_Y := \int_{\mathscr{Y}} \mathrm{d}m, \;\; \hat{J}_Y := \int_{\mathscr{Y}} q_Y q_Y^\top \mathrm{d}m, \;\; \bar{c}_Y := \frac{1}{m_Y}\int_{\mathscr{Y}} q_Y \,\mathrm{d}m. \tag{24}$$

By hypothesis, the center of mass $\bar{c}_Y \in \mathbb{R}^3$ coincides with the geometric center of the yoke which is fixed at the origin of the reference system $\mathcal{F}_\mathrm{Y}$, therefore $\bar{c}_Y = 0$. By introducing the angular speed matrix $\Omega_Y := R_Y^\top \dot{R}_Y = \dot{R}_Y R_Y^\top \in \mathfrak{so}(3)$, we ultimately get

$$K_Y = \frac{1}{2} m_Y \|\dot{q}\|^2 + \frac{1}{2}\mathrm{tr}((\Omega_Y + \Omega_S) R_Y \hat{J}_Y R_Y^\top (\Omega_Y + \Omega_S)^\top). \tag{25}$$

The kinetic energy of the yoke appears to be the sum of two energy contributions. The first term represents the translational kinetic energy of the yoke concentrated in its center. The second term represents the rotational kinetic energy of the yoke. The rotational speed is the sum of the rotational speed of the yoke and that of the shell. The inertia is represented by the quantity $R_Y \hat{J}_Y R_Y^\top$ that represents the inertia tensor of the yoke as seen in the reference system of the shell.

Observation: The matrix R_Y represents a rotation about the x axis of the reference system $\mathcal{F}_Y$, hence it takes the form $\begin{bmatrix} 1 & 0 & 0 \\ 0 & \cos\theta_Y & -\sin\theta_Y \\ 0 & \sin\theta_Y & \cos\theta_Y \end{bmatrix}$. It may be readily verified that $R_Y \Omega_Y = \Omega_Y R_Y$. It is perhaps the case to remark here that the equality $R^\top \dot{R} = \dot{R} R^\top$ holds only under particular circumstance and is not universal. In fact, while the expression $\Omega := R^\top \dot{R}$ defines the angular velocity expressed in the body-fixed reference system, the expression $\Omega^\star := \dot{R} R^\top$ denotes the angular velocity in the inertial reference system. Such angular velocities do not coincide, in general, and are related by the transformation $\Omega^\star = \mathrm{Ad}_R(\Omega)$.

Let q_P denote the coordinate of an infinitesimal volume of mass $\mathrm{d}m$ belonging to the pendulum expressed in the coordinate system $\mathcal{F}_P$. The coordinate of such volume in the inertial reference system is given by $q + R_S R_Y R_P q_P$, hence the kinetic energy of the pendulum expressed in the inertial reference system is given by

$$K_P := \frac{1}{2}\int_{\mathscr{P}} \left\| \frac{\mathrm{d}}{\mathrm{d}t}(q + R_S R_Y R_P q_P) \right\|^2 \mathrm{d}m = \frac{1}{2}\int_{\mathscr{P}} \|\dot{q} + \dot{R}_S R_Y R_P q_P + R_S \dot{R}_Y R_P q_P + R_S R_Y \dot{R}_P q_P\|^2 \mathrm{d}m. \tag{26}$$

Expanding the squared vector norm, we get several terms

$$\begin{aligned} K_P = {} & \frac{1}{2} m_P \|\dot{q}\|^2 + \frac{1}{2}\mathrm{tr}(\dot{R}_S R_Y R_P \hat{J}_P R_P^\top R_Y^\top \dot{R}_S^\top) + \frac{1}{2}\mathrm{tr}(R_S \dot{R}_Y R_P \hat{J}_P R_P^\top \dot{R}_Y^\top R_S^\top) \\ & + \frac{1}{2}\mathrm{tr}(R_S R_Y \dot{R}_P \hat{J}_P \dot{R}_P^\top R_Y^\top R_S^\top) + m_P \dot{q}^\top \dot{R}_S R_Y R_P \bar{c}_P + m_P \dot{q}^\top R_S \dot{R}_Y R_P \bar{c}_P + m_P \dot{q}^\top R_S R_Y \dot{R}_P \bar{c}_P \\ & + \mathrm{tr}(\dot{R}_S R_Y R_P \hat{J}_P R_P^\top \dot{R}_Y^\top R_S^\top) + \mathrm{tr}(\dot{R}_S R_Y R_P \hat{J}_P \dot{R}_P^\top R_Y^\top R_S^\top) + \mathrm{tr}(R_S \dot{R}_Y R_P \hat{J}_P \dot{R}_P^\top R_Y^\top R_S^\top), \end{aligned} \tag{27}$$

where we have used the following constants

$$m_P := \int_{\mathscr{P}} \mathrm{d}m,\ \hat{J}_P := \int_{\mathscr{P}} q_P q_P^\top \mathrm{d}m,\ \bar{c}_P := \frac{1}{m_P}\int_{\mathscr{P}} q_P\,\mathrm{d}m. \tag{28}$$

By introducing the angular speed matrix $\Omega_P := R_P^\top \dot{R}_P = \dot{R}_P R_P^\top \in \mathfrak{so}(3)$, we obtain that the terms related to the rotational kinetic energy sum up as

$$\begin{aligned}
&\frac{1}{2}\mathrm{tr}(\Omega_S(R_Y R_P \hat{J}_P R_P^\top R_Y^\top)\Omega_S^\top) + \frac{1}{2}\mathrm{tr}(\Omega_Y(R_Y R_P \hat{J}_P R_P^\top R_Y^\top)\Omega_Y^\top)\\
&+ \frac{1}{2}\mathrm{tr}((R_Y \Omega_P R_Y^\top)(R_Y R_P \hat{J}_P R_P^\top R_Y^\top)(R_Y \Omega_P^\top R_Y^\top)) + \mathrm{tr}(\Omega_S(R_Y R_P \hat{J}_P R_P^\top R_Y^\top)\Omega_Y^\top)\\
&+ \mathrm{tr}(\Omega_S(R_Y R_P \hat{J}_P R_P^\top R_Y^\top)(R_Y \Omega_P^\top R_Y^\top)) + \mathrm{tr}(\Omega_Y(R_Y R_P \hat{J}_P R_P^\top R_Y^\top)(R_Y \Omega_P^\top R_Y^\top)) =\\
&\frac{1}{2}\mathrm{tr}((\Omega_S + \Omega_Y + R_Y \Omega_P R_Y^\top)(R_Y R_P \hat{J}_P R_P^\top R_Y^\top)(\Omega_S + \Omega_Y + R_Y \Omega_P R_Y^\top)^\top).
\end{aligned} \tag{29}$$

Likewise, the terms related to the position of the center of mass of the pendulum sum up to

$$m_P \dot{q}^\top R_S(\Omega_S + \Omega_Y + R_Y \Omega_P R_Y^\top) R_Y R_P \bar{c}_P, \tag{30}$$

where we notice that, as opposed to previous center-of-mass terms, in this instance it holds that $\bar{c}_P \neq 0$. Therefore, the kinetic energy of the pendulum reads

$$\begin{aligned}
K_P = &\frac{1}{2} m_Y \|\dot{q}\|^2 + m_P \dot{q}^\top R_S(\Omega_S + \Omega_Y + R_Y \Omega_P R_Y^\top) R_Y R_P \bar{c}_P\\
&+ \frac{1}{2}\mathrm{tr}((\Omega_S + \Omega_Y + R_Y \Omega_P R_Y^\top)(R_Y R_P \hat{J}_P R_P^\top R_Y^\top)(\Omega_S + \Omega_Y + R_Y \Omega_P R_Y^\top)^\top).
\end{aligned} \tag{31}$$

In this expression, the first term represents the translational kinetic energy of the pendulum concentrated in its center. The third term represents the rotational kinetic energy of the pendulum in the shell reference system, in fact the inertia matrix of the pendulum is converted to the shell reference system by the expression $R_Y R_P \hat{J}_P R_P^\top R_Y^\top$. The second term in the above sum represents a Coriolis-type virtual energy since it represents the kinetic energy of a moving object observed from the rotating reference system associated to the shell.

2.5. Potential energy of the shell, yoke and pendulum

Since the robot rolls over a horizontal plane, it holds that $q^\top e_z = r$, therefore the center of mass of the shell keeps at a fixed vertical distance r from the ground, hence its potential energy U_S is constant. Such assumption would not be valid for a robot rolling on an inclined plane, for instance. The potential energy U_Y of the yoke is considered to be constant as well. Such assumption is valid as long as one ignores the differences of gravity over the four rods of the yoke which may be at different heights from one another.

The center of mass of the pendulum moves over time as the pendulum itself swings, the yoke oscillates and the shell rolls. The coordinate of the center of mass of the pendulum, expressed in the inertial reference system, is given by $q + R_S R_Y R_P \bar{c}_P$. Hence, the potential energy of the pendulum, in the inertial reference system, reads

$$U_P := m_P g e_z^\top \left(q + R_S R_Y R_P \bar{c}_P\right) = m_P g \left(r + e_z^\top R_S R_Y R_P \bar{c}_P\right), \tag{32}$$

where the constant g denotes the gravitational acceleration.

2.6. Lagrangian function of the spherical robot and reduced Lagrangian

The Lagrangian function $L = L(R_S, R_Y, R_P, \Omega_S, \Omega_Y, \Omega_P, \dot{q})$ associated to the spherical robot is defined as

$$L := K_S + K_Y + K_P - U_S - U_Y - U_P \tag{33}$$

and takes the expression

$$\begin{aligned}
L = &\frac{1}{2} m_R \|R_S^\top \dot{q}\|^2\\
&+ \frac{1}{2}\mathrm{tr}(\Omega_S \hat{J}_R \Omega_S^\top)\\
&+ \frac{1}{2}\mathrm{tr}((\Omega_Y + \Omega_S) R_Y \hat{J}_Y R_Y^\top (\Omega_Y + \Omega_S)^\top)\\
&+ m_P \dot{q}^\top R_S(\Omega_S + \Omega_Y + R_Y \Omega_P R_Y^\top) R_Y R_P \bar{c}_P\\
&+ \frac{1}{2}\mathrm{tr}((\Omega_S + \Omega_Y + R_Y \Omega_P R_Y^\top)(R_Y R_P \hat{J}_P R_P^\top R_Y^\top)(\Omega_S + \Omega_Y + R_Y \Omega_P R_Y^\top)^\top)\\
&- m_P g (R_S^\top e_z)^\top (R_Y R_P \bar{c}_P) + \text{constant},
\end{aligned} \tag{34}$$

where we have defined the total mass content of the robot

$$m_R := m_S + m_Y + m_P \tag{35}$$

and we have made use of the identity $\|R_S^\top \dot{q}\|^2 = \|\dot{q}\|^2$.

A closer look at the terms in the Lagrangian reveals the following:

- the expression $-g R_S^\top e_z$ represents the gravitational acceleration in the reference system $\mathcal{F}_S$ and depends only the matrix R_S, hence, the matrix R_S may be represented, in the Lagrangian, by the new variable $\gamma := R_S^\top e_z$; notice that $\gamma^\top \gamma = 1$, hence $\gamma \in \mathrm{S}^2$,

- likewise, the linear velocity $\dot{q}$ appears only as expressed in the reference system $\mathcal{F}_S$, hence it may be represented by a new variable $v := R_S^\top \dot{q}$; we notice that $\gamma^\top v = 0$, therefore $v \in T_\gamma \mathrm{S}^2$ (namely, in the reference system $\mathcal{F}_S$, the velocity $\dot{q}$ is tangent to the robot surface at the contact point).

The Lagrangian function may hence be written in the new variables. The resulting function is termed *reduced Lagrangian* and is denoted as $\ell = \ell(\gamma, R_Y, R_P, \Omega_S, \Omega_Y, \Omega_P, v)$ and its expression is:

$$\begin{aligned}\ell = & \frac{1}{2} m_R \|v\|^2 \\ & + \frac{1}{2}\mathrm{tr}(\Omega_S \hat{J}_R \Omega_S^\top) + \frac{1}{2}\mathrm{tr}((\Omega_Y + \Omega_S) R_Y \hat{J}_Y R_Y^\top (\Omega_Y + \Omega_S)^\top) \\ & + m_P v^\top (\Omega_S + \Omega_Y + R_Y \Omega_P R_Y^\top) R_Y R_P \bar{c}_P \\ & + \frac{1}{2}\mathrm{tr}((\Omega_S + \Omega_Y + R_Y \Omega_P R_Y^\top)(R_Y R_P \hat{J}_P R_P^\top R_Y^\top)(\Omega_S + \Omega_Y + R_Y \Omega_P R_Y^\top)^\top) \\ & - m_P g \gamma^\top R_Y R_P \bar{c}_P + \text{constant}.\end{aligned} \tag{36}$$

The reduced Lagrangian does not depend explicitly on the orientation of the shell. Such property reflects the fact that the reduced Lagrangian is expressed in the reference system $\mathcal{F}_S$.

(Some authors would introduce the further secondary variable $\xi := R_Y R_P \bar{c}_P \in \frac{l}{2}\mathrm{S}^2$, which represents the position of the center of mass of the pendulum shaft as seen from the yoke-fixed frame $\mathcal{F}_Y$. We do not find such ansatz particularly useful and shall henceforth dispense of it, except that in Appendix B.)

2.7. Non-holonomic constraint and related distribution, advection equation and reduced-constrained Lagrangian

The spherical robot is assumed to roll over a horizontal plane *without slipping*. As a consequence, from the viewpoint of the inertial reference system, the center of mass of the spherical shell rotates instantaneously around the contact point to the ground with angular speed $\mathrm{Ad}_{R_S}(\Omega_S)$. Such property is expressed mathematically through the *non-holonomic* constraint

$$\dot{q} = r R_S \Omega_S R_S^\top e_z. \tag{37}$$

This bound implies that, at a point $(R_S, R_Y, R_P, q) \in \mathbb{Q}$, the state velocity cannot span the whole space $T_{(R_S,R_Y,R_P,q)}\mathbb{Q}$ but its span is confined to a subspace $D_{(R_S,R_Y,R_P,q)}\mathbb{Q}$, whose union forms a so-called *distribution* $D\mathbb{Q} \subset T\mathbb{Q}$. Each element of the distribution has coordinate $(R_S, R_Y, R_P, q; R_S\Omega_S, \dot{R}_Y, \dot{R}_P, r R_S \Omega_S R_S^\top e_z)$.

The non-holonomic constraint may be written in the new set of variables introduced in the previous section by noting that $R_S^\top \dot{q} = r\Omega_S(R_S^\top e_z)$, hence

$$v = r\, \Omega_S\, \gamma. \tag{38}$$

In addition, it is easy to verify that the dynamics of the robot attitude matrix R_S implies the dynamics

$$\dot{\gamma} + \Omega_S \gamma = 0. \tag{39}$$

Such relation is called *advection equation* in the *advected* parameter $\gamma \in \mathrm{S}^2$.

In the new variables, a configuration of the robot is represented by the tuple $(\gamma, R_Y, R_P, q) \in \tilde{\mathbb{Q}}$, while a velocity is represented by the tuple $(\Omega_S, \Omega_Y, \Omega_P, v) \in T_{(\gamma,R_Y,R_P,q)}\tilde{\mathbb{Q}}$. Imposing the constraint (38) leads to a distribution, whose elements are given by $(\gamma, R_Y, R_P, q; \Omega_S, \Omega_Y, \Omega_P, r\Omega_S\gamma) \in D\tilde{\mathbb{Q}}$.

It pays to defined a reduced-constrained Lagrangian function as

$$\ell_c(\gamma, R_Y, R_P, \Omega_S, \Omega_Y, \Omega_P) := \ell(\gamma, R_Y, R_P, \Omega_S, \Omega_Y, \Omega_P, r\Omega_S\gamma). \tag{40}$$

In fact, as it will become apparent later, the equations of dynamics for the studied robot are better expressed in terms of the function ℓ_c. Such reduced-constrained Lagrangian takes the form

$$\begin{aligned}\ell_c = & \frac{1}{2} m_R r^2 \mathrm{tr}(\Omega_S \gamma\gamma^\top \Omega_S^\top) + \frac{1}{2}\mathrm{tr}(\Omega_S \hat{J}_S \Omega_S^\top) + \frac{1}{2}\mathrm{tr}((\Omega_Y + \Omega_S) R_Y \hat{J}_Y R_Y^\top (\Omega_Y + \Omega_S)^\top) \\ & + m_P r \gamma^\top \Omega_S^\top (\Omega_S + \Omega_Y + R_Y \Omega_P R_Y^\top) R_Y R_P \bar{c}_P \\ & + \frac{1}{2}\mathrm{tr}((\Omega_S + \Omega_Y + R_Y \Omega_P R_Y^\top)(R_Y R_P \hat{J}_P R_P^\top R_Y^\top)(\Omega_S + \Omega_Y + R_Y \Omega_P R_Y^\top)^\top) \\ & - m_P g \gamma^\top R_Y R_P \bar{c}_P + \text{constant}.\end{aligned} \tag{41}$$

The unspecified constant term is, of course, of no interest to what will follow.

3. The non-holonomic Lagrange-d'Alembert principle and the non-holonomic Euler-Poincaré equations

The spherical robot, actuated by motors to spin the yoke and the pendulum, is a non-conservative, non-holonomic dynamical system with configuration manifold $\mathbb{Q}$. The equations of motion for such a complex system should enable one to determine the function of time $R_S = R_S(t)$, which describes the orientation of the spherical shell at any observed time and, ultimately, the trajectory of the center of mass of the spherical robot through integration of Eq. (37).

The formulation of the equations of motion is made through an Hamiltonian stationary-action principle, modified by the d'Alembert virtual work principle to accommodate for the non-conservative control inputs as well as energy-dissipative friction, by taking into account the non-holonomic

constraint. The mathematical instruments to achieve such formulation is provided by the calculus of variations on manifolds with variations on the distribution associated with the constraint. The starting point is the variational formulation

$$\underbrace{\delta \int \ell(\gamma, R_Y, R_P, \Omega_S, \Omega_Y, \Omega_P, v)\mathrm{d}t}_{\text{From Hamilton's principle}} + \underbrace{\int (\langle -k_S\Omega_S, \delta\Omega_S\rangle^{\mathfrak{so}(3)} + \langle \tau_Y - k_Y\Omega_Y, \delta\Omega_Y\rangle^{\mathfrak{so}(3)} + \langle \tau_P - k_P\Omega_P, \delta\Omega_P\rangle^{\mathfrak{so}(3)})\mathrm{d}t}_{\text{From d'Alembert virtual work principle}} = 0, \tag{42}$$

where $\langle \star, \star \rangle^{\mathfrak{so}(3)}$ denotes the inner product in $\mathfrak{so}(3)$ and $\tau_Y, \tau_P \in \mathfrak{so}(3)$ denote the mechanical torques exerted by the two electrical motors that handle the yoke and the pendulum, respectively. The constants $k_S > 0$, $k_Y > 0$ and $k_P > 0$ denote braking coefficients due to friction. The resulting equations are termed *non-holonomic Euler–Poincaré equations* [27]. For a high-standing theoretical view of the underlying mathematical principles, interested readers might also consult [28].

In the following sections, we shall derive explicitly the variations indicated in (42). In particular, Section 3.1 recalls briefly how to implement the variational principle, while Sections 3.2 to 3.5 express detailed calculations that lead to an Euler–Poincaré equation for the variable Ω_S, Sections 3.6 and 3.7 deliver the same calculations to get an Euler–Poincaré equation for the variable Ω_Y, while Section 3.8 delivers a similar content for the angular speed Ω_P. Section 3.9 recaps the equations of motion of the studied spherical robot for the convenience of the reader.

3.1. Variational calculus on manifold applied to the spherical robot

The main idea is to define a family of curves in the main variables whose variation induces variations in their dependencies. From the given definitions, we find the following dependencies:

$$\begin{cases} \Omega_S \leftarrow R_S, \\ \Omega_Y \leftarrow R_Y, \\ \Omega_P \leftarrow R_P, \\ \gamma \leftarrow R_S, \\ v \leftarrow \Omega_S \leftarrow R_S, \end{cases} \tag{43}$$

hence the main variables are R_S, R_Y, R_P, a conclusion that matches one's intuition. We shall add to these the positional variable q that will play a secondary role, as it will be explained later.

We shall therefore define families of curves $R_S(t,u)$, $R_Y(t,u)$ and $R_P(t,u)$, where the variable t denotes a point on a curve and the variable u denotes a continuous index which individuates a curve of each family. The optimal curve for each variable R_S, R_Y, R_P corresponds to the index $u = 0$. The variation of the action corresponds to its derivative with respect to the index u at $u = 0$, namely

$$\begin{aligned} \delta \int \ell \,\mathrm{d}t = & \int \left\langle \frac{\partial \ell}{\partial \Omega_S}, \frac{\partial \Omega_S}{\partial u} \right\rangle_{u=0}^{\mathfrak{so}(3)} \mathrm{d}t + \int \left\langle \frac{\partial \ell}{\partial v}, \frac{\partial v}{\partial u} \right\rangle_{u=0}^{\mathbb{R}^3} \mathrm{d}t + \int \left\langle \frac{\partial \ell}{\partial \gamma}, \frac{\partial \gamma}{\partial u} \right\rangle_{u=0}^{\mathbb{R}^3} \mathrm{d}t + \\ & \int \left\langle \frac{\partial \ell}{\partial R_Y}, \frac{\partial R_Y}{\partial u} \right\rangle_{u=0}^{\mathbb{R}^{3\times 3}} \mathrm{d}t + \int \left\langle \frac{\partial \ell}{\partial R_P}, \frac{\partial R_P}{\partial u} \right\rangle_{u=0}^{\mathbb{R}^{3\times 3}} \mathrm{d}t + \\ & \int \left\langle \frac{\partial \ell}{\partial \Omega_Y}, \frac{\partial \Omega_Y}{\partial u} \right\rangle_{u=0}^{\mathfrak{so}(3)} \mathrm{d}t + \int \left\langle \frac{\partial \ell}{\partial \Omega_P}, \frac{\partial \Omega_P}{\partial u} \right\rangle_{u=0}^{\mathfrak{so}(3)} \mathrm{d}t, \end{aligned} \tag{44}$$

where $\langle \star, \star \rangle^{\mathbb{R}^{3\times 3}}$ denotes the Cartesian inner product in the space of 3×3 real-valued matrices and $\langle \star, \star \rangle^{\mathbb{R}^3}$ denotes the Cartesian inner product in the space of 3D real-valued vectors. In the following, we shall be computing each variation independently.

3.2. Expression of the variation $\delta\Omega_S$ induced by a variation δR_S and of the corresponding term in the variation of action

We start off from a family of smooth curves $R_S(t,u)$ with $t \in [0,\ 1]$ and $u \in [-\epsilon,\ \epsilon]$ for some $\epsilon > 0$. Such family is assumed to be smooth, namely such that $\frac{\partial^2 R_S}{\partial t \partial u} = \frac{\partial^2 R_S}{\partial u \partial t}$. In addition, each curve must extend from the same starting point to the same arrival point, namely $R_S(0,u) =$ constant and $R_S(1,u) =$ constant in $[-\epsilon,\ \epsilon]$. We have

$$\Omega_S := R_S^\top \frac{\partial R_S}{\partial t},\ \delta\Omega_S := R_S^\top \frac{\partial R_S}{\partial u}, \tag{45}$$

where the symbol $\delta\Omega_S(t,u)$ denotes a variation of a curve $\Omega_S(\star,u)$ in $\mathfrak{so}(3)$ induced by a variation of a trajectory $R_S(\star,u)$ in the attitude space SO(3). Next, we shall observe that

$$\begin{aligned} \frac{\partial \Omega_S}{\partial u} &= \frac{\partial R_S^\top}{\partial u}\frac{\partial R_S}{\partial t} + R_S^\top \frac{\partial^2 R_S}{\partial u \partial t} = \left(\frac{\partial R_S^\top}{\partial u} R_S\right)\left(R_S^\top \frac{\partial R_S}{\partial t}\right) + R_S^\top \frac{\partial^2 R_S}{\partial u \partial t}, \\ \frac{\partial \delta\Omega_S}{\partial t} &= \frac{\partial R_S^\top}{\partial t}\frac{\partial R_S}{\partial u} + R_S^\top \frac{\partial^2 R_S}{\partial t \partial u} = \left(\frac{\partial R_S^\top}{\partial t} R_S\right)\left(R_S^\top \frac{\partial R_S}{\partial u}\right) + R_S^\top \frac{\partial^2 R_S}{\partial t \partial u}. \end{aligned} \tag{46}$$

The last two addenda of each identity are equal to one another, therefore

$$\frac{\partial \Omega_S}{\partial u} - \frac{\partial \delta\Omega_S}{\partial t} = -\delta\Omega_S\,\Omega_S + \Omega_S\,\delta\Omega_S. \tag{47}$$

In conclusion, it holds that

$$\frac{\partial \Omega_S}{\partial u} = \frac{\partial \delta\Omega_S}{\partial t} + \mathrm{ad}_{\Omega_S}(\delta\Omega_S). \tag{48}$$

The corresponding term in the variation of action reads

$$\int \left\langle \frac{\partial \ell}{\partial \Omega_S}, \frac{\partial \Omega_S}{\partial u} \right\rangle_{u=0}^{\mathfrak{so}(3)} \mathrm{d}t = \int \left\langle \frac{\partial \ell}{\partial \Omega_S}, \frac{\mathrm{d}\delta\Omega_S}{\mathrm{d}t} + \mathrm{ad}_{\Omega_S}(\delta\Omega_S) \right\rangle^{\mathfrak{so}(3)} \mathrm{d}t. \tag{49}$$

The next step consists in expressing the variation of the integral in terms of the variation of the variable Ω_S. By doing so, we get

$$\int \left\langle \left.\frac{\partial \ell}{\partial \Omega_S}\right|_{v=r\Omega_S\gamma}, \frac{\partial \Omega_S}{\partial u} \right\rangle_{u=0}^{\mathfrak{so}(3)} \mathrm{d}t = \int \left\langle -\frac{\mathrm{d}}{\mathrm{d}t}\left(\left.\frac{\partial \ell}{\partial \Omega_S}\right|_{v=r\Omega_S\gamma} \right) + \mathrm{ad}^{\star}_{\Omega_S}\left(\left.\frac{\partial \ell}{\partial \Omega_S}\right|_{v=r\Omega_S\gamma} \right), \delta\Omega_S \right\rangle^{\mathfrak{so}(3)} \mathrm{d}t, \tag{50}$$

where the rule of integration by parts and the dual adjoint operator have been made use of to get to the last expression.

We underline that the sphere is free to roll in virtually every direction, therefore $\Omega_S \in \mathfrak{so}(3)$ and is otherwise unrestricted.

3.3. Expression of the variation $\delta\gamma$ induced by a variation δR_S and of the corresponding term in the variation of action

We start off again from a family of smooth curves $R_S(t,u)$. By definition of the vector-valued function γ, it holds that

$$\frac{\partial \gamma}{\partial u} = \left(\frac{\partial R_S}{\partial u}\right)^{\top} e_z = -\delta\Omega_S\, \gamma. \tag{51}$$

The corresponding term in the variation of action reads

$$\int \left\langle \frac{\partial \ell}{\partial \gamma}, \frac{\partial \gamma}{\partial u} \right\rangle_{u=0}^{\mathbb{R}^3} \mathrm{d}t = -\int \left\langle \frac{\partial \ell}{\partial \gamma}, \delta\Omega_S\, \gamma \right\rangle_{u=0}^{\mathbb{R}^3} \mathrm{d}t. \tag{52}$$

In order to match the other terms in the variation of action, it is convenient to rewrite the latter expression in terms of the inner product in the algebra $\mathfrak{so}(3)$. To this aim, let us notice that $\langle a, b\rangle^{\mathbb{R}^3} = a^{\top} b = \mathrm{tr}(ba^{\top})$, hence

$$\int \left\langle \frac{\partial \ell}{\partial \gamma}, \frac{\partial \gamma}{\partial u} \right\rangle_{u=0}^{\mathbb{R}^3} \mathrm{d}t = -\int \mathrm{tr}\left\{ \delta\Omega_S\, \gamma \left(\frac{\partial \ell}{\partial \gamma}\right)^{\top} \right\} \mathrm{d}t = -\int \left\langle \sigma\left(\frac{\partial \ell}{\partial \gamma}\gamma^{\top}\right), \delta\Omega_S \right\rangle^{\mathfrak{so}(3)} \mathrm{d}t, \tag{53}$$

where we have made use of the projection operator $\sigma(M) := \frac{1}{2}(M - M^{\top})$ which returns a matrix in $\mathfrak{so}(3)$ from any matrix $M \in \mathbb{R}^{3\times 3}$.

An alternative way to express the above term is by introducing the *diamond* operator $\diamond$, defined by

$$a \diamond b := -\sigma(ab^{\top}) = \sigma(ba^{\top}) \tag{54}$$

for all $a, b \in \mathbb{R}^3$, which returns a $\mathfrak{so}(3)$ matrix. The diamond operator may be given an easy interpretation in the $\mathfrak{so}(3)$ case, since it is related to the cross product $\times$ and to the operator $[\![\cdot]\!]$, namely the following equalities hold:

$$[\![a \times b]\!] = [\![[\![a]\!]b]\!] = ab^{\top} - ba^{\top} = -2\sigma(ab^{\top}) = 2\, a \diamond b \tag{55}$$

for any two vectors $a, b \in \mathbb{R}^3$. Hence the diamond operator returns half the skew-symmetric matrix corresponding to the cross product of two $\mathbb{R}^3$ vectors. (Such observation may be utilized to extend the cross product in spaces of dimension higher than three.)

By such notation, the variation (53) takes the form

$$\int \left\langle \left.\frac{\partial \ell}{\partial \gamma}\right|_{v=r\Omega_S\gamma}, \frac{\partial \gamma}{\partial u} \right\rangle_{u=0}^{\mathbb{R}^3} \mathrm{d}t = -\int \left\langle \gamma \diamond \left.\frac{\partial \ell}{\partial \gamma}\right|_{v=r\Omega_S\gamma}, \delta\Omega_S \right\rangle^{\mathfrak{so}(3)} \mathrm{d}t, \tag{56}$$

which takes into account the non-holonomic constraint.

3.4. Expression of the variation δv induced by a variation δR_S and of the corresponding term in the variation of action

While calculating the variation δv, special care must be taken because, as explained in [27], the constraint must be applied only *after* calculating the variation, while an early application would lead to an inconsistent result.

In this instance, we start from a family of smooth curves $R_S(t,u)$ in the attitude space SO(3) and a family of smooth curves $q(t,u)$ in the position space $\mathbb{R}^3$. Such families induce the smooth family of velocities

$$v := R_S^{\top} \frac{\partial q}{\partial t}. \tag{57}$$

The rate of change of the velocity due to a shift to a nearby trajectory reads

$$\frac{\partial v}{\partial u} = \frac{\partial R_S^{\top}}{\partial u}\frac{\partial q}{\partial t} + R_S^{\top}\frac{\partial^2 q}{\partial u \partial t} = -\delta\Omega_S\, v + R_S^{\top}\frac{\partial^2 q}{\partial u \partial t}. \tag{58}$$

In addition, we notice that

$$\frac{\partial}{\partial t}\left(R_S^{\top}\frac{\partial q}{\partial u}\right) = \frac{\partial R_S^{\top}}{\partial t}\frac{\partial q}{\partial u} + R_S^{\top}\frac{\partial^2 q}{\partial t \partial u} = -\Omega_S R_S^{\top}\frac{\partial q}{\partial u} + R_S^{\top}\frac{\partial^2 q}{\partial t \partial u}. \tag{59}$$

The last two addenda in the above two equations are equal to one another, therefore

$$\frac{\partial v}{\partial u} = -\delta\Omega_S\, v + \Omega_S R_S^{\top}\frac{\partial q}{\partial u} + \frac{\partial}{\partial t}\left(R_S^{\top}\frac{\partial q}{\partial u}\right). \tag{60}$$

Such expression stems entirely from the definitions of the variables v, $\delta\Omega_S$ and Ω_S and is hence derived independently of the underlying non-holonomic constraint. To ensure that $\frac{\partial v}{\partial u} \in D\mathbb{Q}$, we shall introduce the constraint in the expression (60). In addition, it is necessary to express the variation $\frac{\partial q}{\partial u}$ induced by a variation in the robot's angular velocity matrix $\delta\Omega_S$. On the basis of the physical meaning of the constraint, such variation is expressed as

$$\frac{\partial q}{\partial u} = r\frac{\partial R_S}{\partial u}\gamma, \tag{61}$$

as already assumed in [27]. The resulting constrained variation of velocity hence reads

$$\frac{\partial v}{\partial u} = -\delta\Omega_S(r\,\Omega_S\gamma) + \Omega_S(r\,\delta\Omega_s\,\gamma) + \frac{\partial}{\partial t}(r\,\delta\Omega_S\,\gamma). \tag{62}$$

Gluing together the first two addenda on the right-hand side by the help of the adjoint endomorphism, we get the final expression

$$\frac{\partial v}{\partial u} = r\frac{\partial}{\partial t}(\delta\Omega_S\gamma) + r\,\mathrm{ad}_{\Omega_S}(\delta\Omega_S)\gamma. \tag{63}$$

The corresponding term in the variation of the action, after plugging in the non-holonomic constraint, reads

$$\begin{aligned}
\int \left\langle \frac{\partial \ell}{\partial v}\Big|_{v=r\Omega_S\gamma}, \frac{\partial v}{\partial u}\right\rangle_{u=0}^{\mathbb{R}^3} \mathrm{d}t &= r\int \left\langle \frac{\partial \ell}{\partial v}\Big|_{v=r\Omega_S\gamma}, \frac{\mathrm{d}}{\mathrm{d}t}(\delta\Omega_S\gamma) + \mathrm{ad}_{\Omega_S}(\delta\Omega_S)\gamma\right\rangle^{\mathbb{R}^3} \mathrm{d}t \\
&= -r\int \left\langle \frac{\mathrm{d}}{\mathrm{d}t}\left(\frac{\partial \ell}{\partial v}\Big|_{v=r\Omega_S\gamma}\right), \delta\Omega_S\gamma\right\rangle^{\mathbb{R}^3} \mathrm{d}t + r\int \left\langle \frac{\partial \ell}{\partial v}\Big|_{v=r\Omega_S\gamma}, \mathrm{ad}_{\Omega_S}(\delta\Omega_S)\gamma\right\rangle^{\mathbb{R}^3} \mathrm{d}t \\
&= -r\int \mathrm{tr}\left\{\delta\Omega_S\gamma\left(\frac{\mathrm{d}}{\mathrm{d}t}\frac{\partial \ell}{\partial v}\Big|_{v=r\Omega_S\gamma}\right)^\top\right\}\mathrm{d}t + r\int \mathrm{tr}\left\{\mathrm{ad}_{\Omega_S}(\delta\Omega_S)\gamma\left(\frac{\partial \ell}{\partial v}\Big|_{v=r\Omega_S\gamma}\right)^\top\right\}\mathrm{d}t \\
= -r\int \left\langle \sigma\left\{\left(\frac{\mathrm{d}}{\mathrm{d}t}\frac{\partial \ell}{\partial v}\Big|_{v=r\Omega_S\gamma}\right)\gamma^\top\right\}, \delta\Omega_S\right\rangle^{\mathfrak{so}(3)} \mathrm{d}t &+ r\int \left\langle \sigma\left(\frac{\partial \ell}{\partial v}\Big|_{v=r\Omega_S\gamma}\gamma^\top\right), \mathrm{ad}_{\Omega_S}(\delta\Omega_S)\right\rangle^{\mathfrak{so}(3)} \mathrm{d}t,
\end{aligned} \tag{64}$$

where we have invoked again the integration-by-part rule and the skew-symmetrizing operator σ. By the help of the diamond operator and of the dual adjoint operator, the above variation may be recast as:

$$\int \left\langle \frac{\partial v}{\partial u}, \frac{\partial \ell}{\partial v}\Big|_{v=r\Omega_S\gamma}\right\rangle_{u=0}^{\mathbb{R}^3} \mathrm{d}t = r\int \left\langle \left(\frac{\mathrm{d}}{\mathrm{d}t}\frac{\partial \ell}{\partial v}\Big|_{v=r\Omega_S\gamma}\right)\diamond\gamma + \mathrm{ad}^\star_{\Omega_S}\left(\gamma\diamond\frac{\partial \ell}{\partial v}\Big|_{v=r\Omega_S\gamma}\right), \delta\Omega_S\right\rangle^{\mathfrak{so}(3)} \mathrm{d}t. \tag{65}$$

3.5. Constrained Euler-Poincaré equation for the angular velocity matrix Ω_S

Since the variation δR_S is arbitrary, it induces an arbitrary variation $\delta\Omega_S$. Taking into account the friction-type term in the master equation (42), the terms computed so far allow writing the Euler–Poincaré equation for the angular velocity matrix Ω_S, that read

$$\begin{aligned}
&\frac{\mathrm{d}}{\mathrm{d}t}\left(\frac{\partial \ell}{\partial \Omega_S}\Big|_{v=r\Omega_S\gamma}\right) - \mathrm{ad}^\star_{\Omega_S}\left(\frac{\partial \ell}{\partial \Omega_S}\Big|_{v=r\Omega_S\gamma}\right) = \\
&\frac{\partial \ell}{\partial \gamma}\Big|_{v=r\Omega_S\gamma}\diamond\gamma + r\left(\frac{\mathrm{d}}{\mathrm{d}t}\frac{\partial \ell}{\partial v}\Big|_{v=r\Omega_S\gamma}\right)\diamond\gamma - r\,\mathrm{ad}^\star_{\Omega_S}\left(\frac{\partial \ell}{\partial v}\Big|_{v=r\Omega_S\gamma}\diamond\gamma\right) - k_S\,\Omega_S.
\end{aligned} \tag{66}$$

The above equation may be expressed more compactly in terms of the constrained Lagrangian ℓ_c. As a first step, let us express the fiber derivative $\frac{\partial \ell}{\partial \Omega_S}$ in terms of the fiber derivative $\frac{\partial \ell_c}{\partial \Omega_S}$. To such aim, let us consider the reduced Lagrangian $\ell(\gamma, R_Y, R_P, \Omega_S, \Omega_Y, \Omega_P, v)$ as a function of seven independent variables, while we consider the reduced-constrained Lagrangian $\ell_c(\gamma, R_Y, R_P, \Omega_S, \Omega_Y, \Omega_P)$, as defined in Section 2.7, as a function of six independent variables. Their relationship, to what matters in the present calculations, reads

$$\ell_c(\gamma, \star, \star, \Omega_S, \star, \star) = \ell(\gamma, \star, \star, \Omega_S, \star, \star, v)|_{v=r\Omega_S\gamma}. \tag{67}$$

The fiber derivative of such functions with respect to the matrix-variable Ω_S arises from their first-order expansion, namely

$$\ell_c(\gamma, \star, \star, \Omega_S + \Delta\Omega_S, \star, \star) = \left\langle \frac{\partial \ell_c}{\partial \Omega_S}, \Delta\Omega_S\right\rangle^{\mathfrak{so}(3)} + \quad \mathscr{O}(\Delta\Omega_S), \tag{68}$$

where $\mathscr{O}(\star)$ denotes the Landau symbol for higher-order infinitesimals. From the relation (67) it follows that

$$\begin{aligned}
\ell_c(\gamma, \star, \star, \Omega_S + \Delta\Omega_S, \star, \star) &= \ell(\gamma, \star, \star, \Omega_S + \Delta\Omega_S, \star, \star, r\Omega_S\gamma + r\Delta\Omega_S\gamma), \\
&= \left\langle \frac{\partial \ell}{\partial \Omega_S}, \Delta\Omega_S\right\rangle_{v=r\Delta\Omega_S\gamma}^{\mathfrak{so}(3)} + \quad \left\langle \frac{\partial \ell}{\partial v}, r\Delta\Omega_S\gamma\right\rangle_{v=r\Delta\Omega_S\gamma}^{\mathbb{R}^3} + \mathscr{O}(\Delta\Omega_S) \\
&= \left\langle \frac{\partial \ell}{\partial \Omega_S}, \Delta\Omega_S\right\rangle_{v=r\Delta\Omega_S\gamma}^{\mathfrak{so}(3)} + \quad r\left\langle \sigma\left(\frac{\partial \ell}{\partial v}\gamma^\top\right), \Delta\Omega_S\right\rangle_{v=r\Delta\Omega_S\gamma}^{\mathfrak{so}(3)} + \mathscr{O}(\Delta\Omega_S).
\end{aligned} \tag{69}$$

Comparing the relations (68) and (69), it is immediate to find that

$$\frac{\partial \ell_c}{\partial \Omega_S} = \frac{\partial \ell}{\partial \Omega_S}\Big|_{v=r\Omega_S\gamma} + r\gamma\diamond\frac{\partial \ell}{\partial v}\Big|_{v=r\Omega_S\gamma}. \tag{70}$$

Such equality may indeed be given an interesting interpretation, which is discussed in Appendix A.

Upon replacing the constrained fiber derivative $\left.\frac{\partial \mathscr{ℓ}}{\partial \Omega_S}\right|_{v=r\Omega_S\gamma}$ in the constrained Euler–Poincaré equation (66) with $\frac{\partial \mathscr{ℓ}_c}{\partial \Omega_S} + r\left.\frac{\partial \mathscr{ℓ}}{\partial v}\right|_{v=r\Omega_S\gamma} \diamond \gamma$, several terms cancel out and the resulting dynamics turn out to be described by

$$\frac{\mathrm{d}}{\mathrm{d}t}\left(\frac{\partial \mathscr{ℓ}_c}{\partial \Omega_S}\right) - \mathrm{ad}^{\star}_{\Omega_S}\left(\frac{\partial \mathscr{ℓ}_c}{\partial \Omega_S}\right) = -\gamma \diamond \left.\frac{\partial \mathscr{ℓ}}{\partial \gamma}\right|_{v=r\Omega_S\gamma} + r\,\dot{\gamma} \diamond \left.\frac{\partial \mathscr{ℓ}}{\partial v}\right|_{v=r\Omega_S\gamma} - k_S\,\Omega_S. \tag{71}$$

Such equation needs to be paired with the so-termed reconstruction equation $\dot{R}_S = R_S\Omega_S$, which allows recovering the trajectory of the robot in the attitude space SO(3) as well as the trajectory of its center of mass, and the advection equation $\dot{\gamma} = -\Omega_S\gamma$.

The constrained Euler–Poincaré equation (71) shows, in the left-hand side, the classical terms in the 'pure' Euler–Poincaré equation, that are essentially due to the inertia of the rolling system, expressed in the shell-fixed reference system. The right-hand side presents forcing terms due to the gravity effects on the pendulum and friction.

3.6. Expression of the variation $\delta\Omega_Y$ induced by a variation δR_Y and of the corresponding term in the variation of action

We shall start with a smooth family of curves $R_Y(t,u)$ and let

$$\Omega_Y := R_Y^{\top}\frac{\partial R_Y}{\partial t},\ \delta\Omega_Y := R_Y^{\top}\frac{\partial R_Y}{\partial u}. \tag{72}$$

Similarly to the case treated in Section 3.2, it is readily found that the rate of change of the angular velocity of the yoke presents the expression

$$\frac{\partial \Omega_Y}{\partial u} = \frac{\partial \delta\Omega_Y}{\partial t} + \mathrm{ad}_{\Omega_Y}(\delta\Omega_Y). \tag{73}$$

The corresponding term in the variation of action reads

$$\int \left\langle \frac{\partial \mathscr{ℓ}}{\partial \Omega_Y}, \frac{\partial \Omega_Y}{\partial u}\right\rangle_{u=0}^{\mathfrak{so}(3)} \mathrm{d}t = \int \left\langle \frac{\partial \mathscr{ℓ}}{\partial \Omega_Y}, \frac{\mathrm{d}\delta\Omega_Y}{\mathrm{d}t} + \mathrm{ad}_{\Omega_Y}(\delta\Omega_Y)\right\rangle^{\mathfrak{so}(3)} \mathrm{d}t. \tag{74}$$

By applying the non-holonomic constraint and expressing the variation of the integral in terms of the variation of the variable Ω_Y, we further get

$$\int \left\langle \left.\frac{\partial \mathscr{ℓ}}{\partial \Omega_Y}\right|_{v=r\Omega_S\gamma}, \frac{\partial \Omega_Y}{\partial u}\right\rangle_{u=0}^{\mathfrak{so}(3)} \mathrm{d}t = \int \left\langle -\frac{\mathrm{d}}{\mathrm{d}t}\left(\frac{\partial \mathscr{ℓ}_c}{\partial \Omega_Y}\right) + \mathrm{ad}^{\star}_{\Omega_Y}\left(\frac{\partial \mathscr{ℓ}_c}{\partial \Omega_Y}\right), \delta\Omega_Y\right\rangle^{\mathfrak{so}(3)} \mathrm{d}t, \tag{75}$$

where the rule of integration by parts and the dual adjoint endomorphism have been made use of to get to the last expression and the observation that the fiber derivative of the reduced Lagrangian and of the constrained-reduced Lagrangian, in the present case, coincide with one another.

We underline that the yoke is free to swing only around the x axis in its own reference system, therefore $\Omega_Y \in \mathrm{span}\{\Sigma_Y\} \subset \mathfrak{so}(3)$.

3.7. Other terms related to the variation δR_Y and corresponding Euler-Poincaré equation

There exist two further terms in the master equation (42) related to the variation δR_Y. The first one may be expressed as

$$\begin{aligned}\int \left\langle \left.\frac{\partial \mathscr{ℓ}}{\partial R_Y}\right|_{v=r\Omega_S\gamma}, \frac{\partial R_Y}{\partial u}\right\rangle_{u=0}^{\mathbb{R}^{3\times3}} \mathrm{d}t &= \int \left\langle \frac{\partial \mathscr{ℓ}_c}{\partial R_Y}, R_Y\,\delta\Omega_Y\right\rangle_{u=0}^{\mathbb{R}^{3\times3}} \mathrm{d}t \\ &= \int \mathrm{tr}\left\{\left(\frac{\partial \mathscr{ℓ}_c}{\partial R_Y}\right)^{\top} R_Y\,\delta\Omega_Y\right\} \mathrm{d}t \\ &= \int \left\langle \sigma_Y\left\{R_Y^{\top}\frac{\partial \mathscr{ℓ}_c}{\partial R_Y}\right\}, \delta\Omega_Y\right\rangle^{\mathfrak{so}(3)} \mathrm{d}t,\end{aligned} \tag{76}$$

where $\sigma_Y : \mathbb{R}^{3\times3} \to \mathrm{span}\{\Sigma_Y\}$ denotes an orthogonal projector over the subspace of the algebra $\mathfrak{so}(3)$ spanned by yoke's angular speeds, namely $\sigma_Y(M) := \frac{1}{2}\mathrm{tr}(M^{\top}\Sigma_Y)\Sigma_Y$. (The factor $\frac{1}{2}$ arises from the observation that $\mathrm{tr}(\Sigma_Y^{\top}\Sigma_Y) = 2$.)

The last term involving the variation $\delta\Omega_Y$ corresponds to the virtual work of the mechanical torque τ_Y and to the friction, namely

$$\int \langle \tau_Y - k_Y\Omega_Y, \delta\Omega_Y\rangle^{\mathfrak{so}(3)}\mathrm{d}t, \tag{77}$$

where, by the physical construction of the spherical robot, it holds that $\tau_Y \in \mathrm{span}\{\Sigma_Y\}$.

It pays to notice now that, since both Ω_Y and $\frac{\partial \mathscr{ℓ}_c}{\partial \Omega_Y}$ are parallel to Σ_Y, it turns out that $\mathrm{ad}_{\Omega_Y}\left(\frac{\partial \mathscr{ℓ}_c}{\partial \Omega_Y}\right) = 0$. Therefore, the dynamics of the yoke is described by the constrained Euler–Poincaré equation

$$\frac{\mathrm{d}}{\mathrm{d}t}\left(\frac{\partial \mathscr{ℓ}_c}{\partial \Omega_Y}\right) - \sigma_Y\left(R_Y^{\top}\frac{\partial \mathscr{ℓ}_c}{\partial R_Y}\right) = \tau_Y - k_Y\,\Omega_Y. \tag{78}$$

Such relation may be paired with the reconstruction equation $\dot{R}_Y = R_Y\Omega_Y$, which allows recovering the trajectory of the yoke in the attitude space SO(3). (The absolute attitude of the yoke in the inertial reference system is represented by the product $R_S R_Y$.)

3.8. Expression of the variation $\delta\Omega_P$ induced by a variation δR_P, corresponding terms in the master equation and corresponding Euler-Poincaré equation

In this instance of the current variational analysis, we shall start with a smooth family of curves $R_P(t,u)$ and let

$$\Omega_P := R_P^{\top}\frac{\partial R_P}{\partial t},\ \delta\Omega_P := R_P^{\top}\frac{\partial R_P}{\partial u}. \tag{79}$$

Similarly to the cases treated in the previous sections, the rate of change of the angular velocity of the pendulum component reads

$$\frac{\partial \Omega_P}{\partial u} = \frac{\partial \delta\Omega_P}{\partial t} + \mathrm{ad}_{\Omega_P}(\delta\Omega_P). \tag{80}$$

Applying the non-holonomic constraint and expressing the variation of the integral in terms of the variation of the matrix variable Ω_P, the corresponding term in the variation of the action is found to take the expression

$$\int \left\langle \left.\frac{\partial \ell}{\partial \Omega_P}\right|_{v=r\Omega_S\gamma}, \frac{\partial \Omega_P}{\partial u} \right\rangle_{u=0}^{\mathfrak{so}(3)} \mathrm{d}t = \int \left\langle -\frac{\mathrm{d}}{\mathrm{d}t}\left(\frac{\partial \ell_c}{\partial \Omega_P}\right) + \mathrm{ad}^{\star}_{\Omega_P}\left(\frac{\partial \ell_c}{\partial \Omega_P}\right), \delta\Omega_P \right\rangle^{\mathfrak{so}(3)} \mathrm{d}t. \tag{81}$$

A further term in the master equation (42) related to the variation δR_P reads

$$\begin{aligned} \int \left\langle \left.\frac{\partial \ell}{\partial R_P}\right|_{v=r\Omega_P\gamma}, \frac{\partial R_P}{\partial u} \right\rangle_{u=0}^{\mathbb{R}^{3\times 3}} \mathrm{d}t &= \int \left\langle \frac{\partial \ell_c}{\partial R_P}, R_P\,\delta\Omega_P \right\rangle_{u=0}^{\mathbb{R}^{3\times 3}} \mathrm{d}t \\ &= \int \mathrm{tr}\left\{ \left(\frac{\partial \ell_c}{\partial R_P}\right)^{\top} R_P\,\delta\Omega_P \right\} \mathrm{d}t \\ &= \int \left\langle \sigma_P\left\{ R_P^{\top}\frac{\partial \ell_c}{\partial R_P}\right\}, \delta\Omega_P \right\rangle^{\mathfrak{so}(3)} \mathrm{d}t, \end{aligned} \tag{82}$$

where $\sigma_P : \mathbb{R}^{3\times 3} \to \mathrm{span}\{\Sigma_P\}$ denotes an orthogonal projector over the subspace of the algebra $\mathfrak{so}(3)$ spanned by pendulum's angular velocity, namely $\sigma_P(M) := \frac{1}{2}\mathrm{tr}(M^{\top}\Sigma_P)\Sigma_P$. In addition, we take into account the virtual work of the mechanical torque exerted on the pendulum by the connected motor and of the friction

$$\int \langle \tau_P - k_P\Omega_P, \delta\Omega_P\rangle^{\mathfrak{so}(3)} \mathrm{d}t, \tag{83}$$

where $\tau_P \in \mathrm{span}\{\Sigma_P\}$ by mechanical construction.

Even in this case, it pays to notice that $\mathrm{ad}_{\Omega_P}\left(\frac{\partial \ell_c}{\partial \Omega_P}\right) = 0$. Therefore, the dynamics of the pendulum is described by the constrained Euler–Poincaré equation

$$\frac{\mathrm{d}}{\mathrm{d}t}\left(\frac{\partial \ell_c}{\partial \Omega_P}\right) - \sigma_P\left(R_P^{\top}\frac{\partial \ell_c}{\partial R_P}\right) = \tau_P - k_P\,\Omega_P. \tag{84}$$

Such equation, once paired with the reconstruction relation $\dot{R}_P = R_P\Omega_P$, allows reconstructing the trajectory of the pendulum in the attitude space SO(3). (The absolute position of the center of mass of the counter-weight pendulum is given by the expression $R_S R_Y R_P \bar{c}_P$, while the absolute position of the free tip of the pendulum shaft in the inertial reference system is given by $-lR_S R_Y R_P e_z$.)

We shall notice that it is possible, and sometimes convenient, to represent the pendulum swinging velocity in the yoke frame, hence giving rise to a special representation of the equations of motion. Such representation is detailed in Appendix B.

3.9. Complete mathematical model of the spherical robot

For the sake of clarity, we gather in the following the six equations in the six independent variables that describe completely the rolling motion of the studied spherical robot:

$$\begin{cases} \frac{\mathrm{d}}{\mathrm{d}t}\left(\frac{\partial \ell_c}{\partial \Omega_S}\right) - \mathrm{ad}^{\star}_{\Omega_S}\left(\frac{\partial \ell_c}{\partial \Omega_S}\right) = -\gamma \diamond \left.\frac{\partial \ell}{\partial \gamma}\right|_{v=r\Omega_S\gamma} + r\dot{\gamma} \diamond \left.\frac{\partial \ell}{\partial v}\right|_{v=r\Omega_S\gamma} - k_S\,\Omega_S, \\ \frac{\mathrm{d}}{\mathrm{d}t}\left(\frac{\partial \ell_c}{\partial \Omega_Y}\right) - \sigma_Y\left(R_Y^{\top}\frac{\partial \ell_c}{\partial R_Y}\right) = \tau_Y - k_Y\,\Omega_Y, \\ \frac{\mathrm{d}}{\mathrm{d}t}\left(\frac{\partial \ell_c}{\partial \Omega_P}\right) - \sigma_P\left(R_P^{\top}\frac{\partial \ell_c}{\partial R_P}\right) = \tau_P - k_P\,\Omega_P, \\ \dot{R}_Y = R_Y\Omega_Y, \\ \dot{\gamma} + \Omega_S\gamma = 0, \\ \dot{R}_P = R_P\Omega_P. \end{cases} \tag{85}$$

It should be remarked that each group of equations are referred to a specific reference system (either the one fixed with the shell, the yoke and the pendulum) and the torques are hence supposed to be expressed with reference to such frames. The Table 1 presents a breakdown of the terms that appear in the equations of motion (85) together with a short description of their mechanical meaning.

Next to such equations there stand the reconstruction formulas

$$\begin{cases} \dot{R}_S = R_S\Omega_S, \\ \dot{q} = r\dot{R}_S\gamma, \end{cases} \tag{86}$$

through which it is possible to determine the position of the geometric center of the robot and its orientation at any time.

It is interesting to remark that the control inputs do not influence directly the motion of the shell, that is indirectly determined by the action of the yoke and of the pendulum which, in turn, respond to the control inputs. It is also worth underlying that the variables Ω_S, Ω_Y, Ω_P, γ and q evolve on vector spaces ($\mathfrak{so}(3)$ and $\mathbb{R}^3$), hence the differential equations governing their evolution over time may be solved numerically through conventional recipes. Conversely, the variables R_S, R_Y and R_P evolve on curved spaces, hence their approximate calculation call for specific numerical recipes [29].

Table 1
A breakdown of the terms in (85) with a short description of their interpretation.

Term	Rational-mechanical interpretation
$\frac{\partial \ell_c}{\partial \Omega_S}$	Generalized angular momentum associated to the rotational motion of the sphere
$\mathrm{ad}^{\star}_{\Omega_S}\left(\frac{\partial \ell_c}{\partial \Omega_S}\right)$	Axicentrifugal torque due to lack of balance of mass distribution within a body
$-\gamma \diamond \frac{\partial \ell}{\partial \gamma}\Big\|_{v=r\Omega_S\gamma}$	Reaction torque on the shell exerted by the motion of the yoke and the pendulum
$r\dot{\gamma} \diamond \frac{\partial \ell}{\partial v}\Big\|_{v=r\Omega_S\gamma}$	Coriolis-type (apparent) torque due to relative rotation
$-k_S\Omega_S$	Braking torque on the spherical shell due to friction
$\frac{\partial \ell_c}{\partial \Omega_Y}$	Generalized angular momentum associated to the swinging motion of the yoke
$\sigma_Y\left(R_Y^\top \frac{\partial \ell_c}{\partial R_Y}\right)$	Reaction torque on the yoke exerted by the shell and the pendulum
$-k_Y\Omega_Y$	Braking torque on the yoke frame due to friction
$\frac{\partial \ell_c}{\partial \Omega_P}$	Generalized angular momentum associated to the oscillatory motion of the pendulum
$\sigma_P\left(R_P^\top \frac{\partial \ell_c}{\partial R_P}\right)$	Reaction torque on the pendulum shaft exerted by the shell and the yoke
$-k_P\Omega_P$	Braking torque on the pendulum shaft due to friction

3.10. An alternative way to approach the modeling problem

Application of the Lagrange–d'Alembert principle together with a Lagrangian function is a widely used and time-proved procedure. Another principle concerning nonholonomic systems (with conditions in the first and possibly in the higher time derivatives) is the Appell–Gibbs approach. Such principle is based on velocities rather than displacements and its combination with the virtual work principle seems possible. Such an approach is potentially able to provide a transparent formulation of the governing systems. For a recent review of this matter, readers might consult [30].

In principle, both approaches lead to the identical analytic results. However, the Appell–Gibbs formulation has a potential to make the analysis itself easier and to enable some "side steps" often providing physically interesting results, which are rather complicated to be achieved by means of a conventional way.

4. Detailed calculations

The next step consists in computing explicitly the derivatives of the Lagrangian functions with respect to the independent variables, which is accomplished in Sections 4.1 and 4.2 below. All derivatives are computed with reference to the inner products defined in the spaces that they belong to. In addition, Section 4.3 derives the equilibrium points of the robots from purely geometric considerations.

4.1. Calculation of the derivatives of the Lagrangian

The fiber derivative of the reduced-constrained Lagrangian (41) with respect to the angular velocity matrix of the spherical shell reads

$$\begin{aligned}\frac{\partial \ell_c}{\partial \Omega_S} = \sigma\{&(m_R r^2 \gamma\gamma^\top + \hat{J}_S + R_Y \hat{J}_Y R_Y^\top + R_Y R_P \hat{J}_P R_P^\top R_Y^\top + \\ &m_P r(\gamma \bar{c}_P^\top R_P^\top R_Y^\top + R_Y R_P \bar{c}_P \gamma^\top))\Omega_S + \\ &(R_Y \hat{J}_Y R_Y^\top + R_Y R_P \hat{J}_P R_P^\top R_Y^\top + m_P r\gamma \bar{c}_P^\top R_P^\top R_Y^\top)\Omega_Y + \\ &(R_Y R_P \hat{J}_P R_P^\top R_Y^\top + m_P r\gamma \bar{c}_P^\top R_P^\top R_Y^\top) R_Y \Omega_P R_Y^\top\}.\end{aligned} \tag{87}$$

Such fiber derivative takes the form of a linear combination of the angular-velocity matrices Ω_S, Ω_Y and Ω_P. The configuration-dependent matrix-coefficients of such combination possess a well-recognizable rational-mechanical meaning. For example, the symmetric, 3×3 matrix-type coefficient $m_R r^2 \gamma\gamma^\top + \hat{J}_S + R_Y \hat{J}_Y R_Y^\top + R_Y R_P \hat{J}_P R_P^\top R_Y^\top + m_P r(\gamma \bar{c}_P^\top R_P^\top R_Y^\top + R_Y R_P \bar{c}_P \gamma^\top)$ is readily interpreted as a generalized, inertia tensor that takes into account all moving constituents of the robot, expressed in the reference system of the spherical shell.

Due to the complex structure of the robot and to the chosen Lie-group/Lie-algebra representation, the inertia of this mechanical system is not represented by a matrix but as a linear operator, as will be shown in Section 4.2.

The derivative of the reduced Lagrangian with respect to the advected parameter-vector reads

$$\left.\frac{\partial \ell}{\partial \gamma}\right|_{v=r\Omega_S\gamma} = -m_P g R_Y R_P \bar{c}_P. \tag{88}$$

As a consequence, the term in the relation (71) that involves such derivative presents the expression

$$-\gamma \diamond \left.\frac{\partial \ell}{\partial \gamma}\right|_{v=r\Omega_S\gamma} = m_P g \sigma(R_Y R_P \bar{c}_P \gamma^\top). \tag{89}$$

Table 2
Vanishing conditions of some torques and their rational-mechanical interpretation.

Expression	Vanishing condition and interpretation
(89)	$R_Y R_P \bar{c}_P \parallel \gamma$, it indicates that the pendulum shaft is parallel to the direction of gravity as seen from the shell reference system
(91)	$\dot{\gamma} = 0$, it is satisfied when the spherical shell is still (while other parts may be moving)
(94)	$\Omega_S = \Omega_Y = \Omega_P = 0$ and $R_P \bar{c}_P \parallel R_Y^\top \gamma$, it indicates that both the three moving parts are still and the pendulum shaft is parallel to the direction of gravity as seen from the yoke reference system
(95)	$\Omega_S = \Omega_Y = \Omega_P = 0$ and $R_P^\top R_Y^\top \gamma \parallel \bar{c}_P$, it indicates that both the three moving parts are still and the pendulum shaft is parallel to the direction of gravity as seen from the pendulum reference system

The derivative of the reduced Lagrangian with respect to the velocity of the center of the sphere, in the shell-fixed reference system, reads

$$\left.\frac{\partial \ell}{\partial v}\right|_{v=r\Omega_S\gamma} = \Omega_S(m_R r\gamma + m_P R_Y R_P \bar{c}_P) + \Omega_Y(m_P R_Y R_P \bar{c}_P) + R_Y \Omega_P (m_P R_P \bar{c}_P). \tag{90}$$

We notice that this term is similar to the corresponding one presented in [31], although the coefficient of the shell's angular velocity Ω_S presents an extra term arising from the non-holonomic constraint. The term in the Euler–Poincaré equation (71) corresponding to the above derivative presents the expression

$$\begin{aligned}\dot{\gamma} \diamond \left.\frac{\partial \ell}{\partial v}\right|_{v=r\Omega_S\gamma} = \sigma\{&\dot{\gamma}(m_R r\gamma + m_P R_Y R_P \bar{c}_P)^\top \Omega_S + \dot{\gamma}(m_P R_Y R_P \bar{c}_P)^\top \Omega_Y + \\ &\dot{\gamma}(m_P R_Y R_P \bar{c}_P)^\top R_Y \Omega_P R_Y^\top\}.\end{aligned} \tag{91}$$

The fiber derivative of the reduced-constrained Lagrangian with respect to the angular velocity matrix of the yoke takes the expression

$$\begin{aligned}\frac{\partial \ell_c}{\partial \Omega_Y} = \sigma_Y\{&(R_Y \hat{J}_Y R_Y^\top + R_Y R_P \hat{J}_P R_P^\top R_Y^\top + m_P r R_Y R_P \bar{c}_P \gamma^\top)\Omega_S + \\ &(R_Y \hat{J}_Y R_Y^\top + R_Y R_P \hat{J}_P R_P^\top R_Y^\top)\Omega_Y + (R_Y R_P \hat{J}_P R_P^\top R_Y^\top) R_Y \Omega_P R_Y^\top\}.\end{aligned} \tag{92}$$

Likewise, the fiber derivative of the reduced-constrained Lagrangian with respect to the angular velocity matrix of the counter-weight pendulum takes the expression

$$\frac{\partial \ell_c}{\partial \Omega_P} = \sigma_P\{R_Y^\top(\Omega_S(R_Y R_P \hat{J}_P + m_P r\gamma \bar{c}_P^\top) + \Omega_Y(R_Y R_P \hat{J}_P) + R_Y \Omega_P R_Y^\top (R_Y R_P \hat{J}_P)) R_P^\top\}. \tag{93}$$

Next, it is necessary to compute the partial derivative of the reduced-constrained Lagrangian with respect to the attitude matrix of the yoke, which reads

$$\begin{aligned}\frac{\partial \ell_c}{\partial R_Y} = &(\Omega_S + \Omega_Y)^\top (\Omega_S + \Omega_Y) R_Y \hat{J}_Y + \\ &(\Omega_S + \Omega_Y + R_Y \Omega_P R_Y^\top) R_Y R_P \hat{J}_P R_P^\top \Omega_P^\top + \\ &R_Y R_P \hat{J}_P R_P^\top R_Y^\top (\Omega_S + \Omega_Y + R_Y \Omega_P R_Y^\top) R_Y \Omega_P + \\ &(\Omega_S + \Omega_Y + R_Y \Omega_P R_Y^\top)^\top (\Omega_S + \Omega_Y + R_Y \Omega_P R_Y^\top) R_Y R_P \hat{J}_P R_P^\top + \\ &m_P r \Omega_S \gamma \bar{c}_P^\top R_P^\top \Omega_P^\top + m_P r R_Y R_P \bar{c}_P \gamma^\top \Omega_S^\top R_Y \Omega_P + \\ &m_P r (\Omega_S + \Omega_Y + R_Y \Omega_P R_Y^\top)^\top \Omega_S \gamma \bar{c}_P^\top R_P^\top - m_P g \gamma \bar{c}_P^\top R_P^\top.\end{aligned} \tag{94}$$

Likewise, it is necessary to calculate the partial derivative of the reduced-constrained Lagrangian with respect to the attitude matrix of the pendulum, which reads

$$\begin{aligned}\frac{\partial \ell_c}{\partial R_P} = &R_Y^\top (\Omega_S + \Omega_Y + R_Y \Omega_P R_Y^\top)^\top (\Omega_S + \Omega_Y + R_Y \Omega_P R_Y^\top) R_Y R_P \hat{J}_P + \\ &m_P r R_Y^\top (\Omega_S + \Omega_Y + R_Y \Omega_P R_Y^\top)^\top \Omega_S \gamma \bar{c}_P^\top - m_P g R_Y^\top \gamma \bar{c}_P^\top.\end{aligned} \tag{95}$$

It is perhaps instructive to check in which configuration of the robot the above-calculated quantities vanish to zero, as this exercise helps getting a glimpse of the mechanical meaning of such terms. Such exercise is conducted in the Table 2.

4.2. Time-derivatives of the fiber derivatives

Each fiber derivative of the reduced-constrained Lagrangian in (85) may be interpreted as a generalized angular momentum in $\mathfrak{so}(3)$, namely

$$\Lambda_S := \frac{\partial \ell_c}{\partial \Omega_S}, \ \Lambda_Y := \frac{\partial \ell_c}{\partial \Omega_Y}, \ \Lambda_P := \frac{\partial \ell_c}{\partial \Omega_P}. \tag{96}$$

It is important to keep in mind that, even though such angular momenta belong formally to the same space, the Lie algebra associated to the group of three-dimensional rotations, they may not be compared directly, because each of them is referred to a different reference system.

The generalized angular momenta are related to the angular velocities and to the instantaneous internal state of the robot by the relationship

$$\begin{bmatrix} \Lambda_S \\ \Lambda_Y \\ \Lambda_P \end{bmatrix} = \mathbb{J} \begin{bmatrix} \Omega_S \\ \Omega_Y \\ \Omega_P \end{bmatrix}, \tag{97}$$

where $\mathbb{J} : (\mathfrak{so}(3))^3 \to (\mathfrak{so}(3))^3$ denotes a generalized inertia operator that depends on the attitude of the yoke and of the pendulum as well as on the attitude of the shell via the 'rotated gravity' direction γ. Complex mechanical systems, which include several components that moves with respect to each others, are described by generalized, state-dependent inertia tensors (or mass tensors) [32]. The generalized inertia operator reads

$$\mathbb{J} := \begin{bmatrix} \sigma(J_{SS}\,\bullet) & \sigma(J_{SY}\,\bullet) & \sigma(J_{SP}\,\bullet\,R_Y^\top) \\ \sigma_Y(J_{YS}\,\bullet) & \sigma_Y(J_{YY}\,\bullet) & \sigma_Y(J_{YP}\,\bullet\,R_Y^\top) \\ \sigma_P(J_{PS}\,\bullet\,R_Y) & \sigma_P(J_{PY}\,\bullet\,R_Y) & \sigma_P(J_{PP}\,\bullet) \end{bmatrix}, \tag{98}$$

where the bullet $\bullet$ denotes a placeholder for the corresponding angular velocity. The state-dependent inertia matrices in (98) take the expressions

$$\begin{cases} J_{SS} := m_R r^2 \gamma\gamma^\top + \hat{J}_S + R_Y \hat{J}_Y R_Y^\top + R_Y R_P \hat{J}_P R_P^\top R_Y^\top + m_P r(\gamma \bar{c}_P^\top R_P^\top R_Y^\top + R_Y R_P \bar{c}_P \gamma^\top), \\ J_{SY} := R_Y \hat{J}_Y R_Y^\top + R_Y R_P \hat{J}_P R_P^\top R_Y^\top + m_P r \gamma \bar{c}_P^\top R_P^\top R_Y^\top, \\ J_{SP} := (R_Y R_P \hat{J}_P + m_P r \gamma \bar{c}_P^\top) R_P^\top, \\ J_{YS} := J_{SY}^\top, \\ J_{YY} := R_Y (\hat{J}_Y + R_P \hat{J}_P R_P^\top) R_Y^\top, \\ J_{YP} := R_Y R_P \hat{J}_P R_P^\top, \\ J_{PS} := J_{SP}^\top, \\ J_{PY} := J_{YP}^\top, \\ J_{PP} := R_P \hat{J}_P R_P^\top. \end{cases} \tag{99}$$

The above inertia matrices present a number of repeated terms: such redundancy may be exploited to simplify their expressions and their calculation on a computing platform.

The generalized inertia operator $\mathbb{J}$ enjoys an important property, as shown in the following.

Lemma 1. *The generalized inertia operator $\mathbb{J}$ is positive-definite over the space $\mathfrak{so}(3)$.*

Proof. The reduced-constrained kinetic energy of the spherical robot reads

$$\begin{aligned} k_c := & \frac{1}{2} m_R r^2 \mathrm{tr}(\Omega_S \gamma\gamma^\top \Omega_S^\top) + \frac{1}{2} \mathrm{tr}(\Omega_S \hat{J}_S \Omega_S^\top) + \frac{1}{2} \mathrm{tr}((\Omega_Y + \Omega_S) R_Y \hat{J}_Y R_Y^\top (\Omega_Y + \Omega_S)^\top) \\ & + m_P r \gamma^\top \Omega_S^\top (\Omega_S + \Omega_Y + R_Y \Omega_P R_Y^\top) R_Y R_P \bar{c}_P \\ & + \frac{1}{2} \mathrm{tr}((\Omega_S + \Omega_Y + R_Y \Omega_P R_Y^\top)(R_Y R_P \hat{J}_P R_P^\top R_Y^\top)(\Omega_S + \Omega_Y + R_Y \Omega_P R_Y^\top)^\top). \end{aligned} \tag{100}$$

Since it is defined as a sum of three non-negative quadratic forms, it is a positive function except when $\Omega_S = \Omega_Y = \Omega_P = 0$. On the other side, it is easy to verify directly that

$$k_c = \tfrac{1}{2} \mathrm{tr}(\Omega^\top \mathbb{J} \Omega), \tag{101}$$

hence the assertion follows. □

The Euler–Poincaré equations in (85) are based on the time-derivative of such generalized momenta, namely $\frac{\mathrm{d}\Lambda_S}{\mathrm{d}t}$, $\frac{\mathrm{d}\Lambda_Y}{\mathrm{d}t}$ and $\frac{\mathrm{d}\Lambda_P}{\mathrm{d}t}$. On the basis of the expressions (97), we can make use of the compact expression

$$\begin{bmatrix} \dot{\Lambda}_S \\ \dot{\Lambda}_Y \\ \dot{\Lambda}_P \end{bmatrix} = \mathbb{J} \begin{bmatrix} \dot{\Omega}_S \\ \dot{\Omega}_Y \\ \dot{\Omega}_P \end{bmatrix} + \dot{\mathbb{J}} \begin{bmatrix} \Omega_S \\ \Omega_Y \\ \Omega_P \end{bmatrix}, \tag{102}$$

which resembles the second equation of dynamics of newton that relates the rate of change of the angular momentum to the applied torque in the case of a multi-body object with variable inertia. The time-derivative of the generalized inertia operator reads

$$\dot{\mathbb{J}} = \begin{bmatrix} \sigma(\dot{J}_{SS}\,\bullet) & \sigma(\dot{J}_{SY}\,\bullet) & \sigma(\dot{J}_{SP}\,\bullet\,R_Y^\top + J_{SP}\,\bullet\,\dot{R}_Y^\top) \\ \sigma_Y(\dot{J}_{YS}\,\bullet) & \sigma_Y(\dot{J}_{YY}\,\bullet) & \sigma_Y(\dot{J}_{YP}\,\bullet\,R_Y^\top + J_{YP}\,\bullet\,\dot{R}_Y^\top) \\ \sigma_P(\dot{J}_{PS}\,\bullet\,R_Y + J_{PS}\,\bullet\,\dot{R}_Y) & \sigma_P(\dot{J}_{PY}\,\bullet\,R_Y + J_{PY}\,\bullet\,\dot{R}_Y) & \sigma_P(\dot{J}_{PP}\,\bullet) \end{bmatrix}. \tag{103}$$

The time-derivative of the variable inertia coefficients are evaluated on the basis of their definitions (99). For example, we have

$$\dot{J}_{PP} = \dot{R}_P \hat{J}_P R_P^\top + R_P \hat{J}_P \dot{R}_P^\top = R_P (\Omega_P \hat{J}_P - \hat{J}_P \Omega_P) R_P^\top. \tag{104}$$

As opposed to the inertia operator $\mathbb{J}$, its time derivative $\dot{\mathbb{J}}$ is not linear in the angular velocity matrices.

By virtue of Lemma 1, the generalized inertia operator is invertible. From the expression (102), by inversion it is possible to determine the angular accelerations $\dot{\Omega}_S$, $\dot{\Omega}_Y$ and $\dot{\Omega}_P$ as

$$\begin{bmatrix} \dot{\Omega}_S \\ \dot{\Omega}_Y \\ \dot{\Omega}_P \end{bmatrix} = \mathbb{J}^{-1} \left\{ \begin{bmatrix} \mathrm{ad}^\star_{\Omega_S} \left(\frac{\partial \ell_c}{\partial \Omega_S} \right) - \gamma \diamond \left. \frac{\partial \ell}{\partial \gamma} \right|_{v = r\Omega_S \gamma} + r\dot{\gamma} \diamond \left. \frac{\partial \ell}{\partial v} \right|_{v = r\Omega_S \gamma} - k_S \Omega_S \\ \sigma_Y \left(R_Y^\top \frac{\partial \ell_c}{\partial R_Y} \right) + \tau_Y - k_Y \Omega_Y \\ \sigma_P \left(R_P^\top \frac{\partial \ell_c}{\partial R_P} \right) + \tau_P - k_P \Omega_P \end{bmatrix} - \dot{\mathbb{J}} \begin{bmatrix} \Omega_S \\ \Omega_Y \\ \Omega_P \end{bmatrix} \right\}, \tag{105}$$

from which the values of the angular velocities may be determined by numerical integration. Since the operator $\mathbb{J}$ is linear in its three $\mathfrak{so}(3)$-valued arguments, the inverse operator $\mathbb{J}^{-1}$ may be computed by linear algebra tools, as detailed in Appendix C.

4.3. Configurations of equilibrium

Any configuration at equilibrium is characterized by null angular velocities, namely $\Omega_S = \Omega_Y = \Omega_P = 0$, and angular accelerations $\dot{\Omega}_S = \dot{\Omega}_Y = \dot{\Omega}_P = 0$ and constant holding torques τ_Y, τ_P. Under these conditions, the equations of motion (85) become

$$\begin{cases} \gamma \diamond \left.\frac{\partial \ell}{\partial \gamma}\right|_{v=r\Omega_S \gamma} = 0, \\ \sigma_Y \left(R_Y^\top \frac{\partial \ell_c}{\partial R_Y} \right) + \tau_Y = 0, \\ \sigma_P \left(R_P^\top \frac{\partial \ell_c}{\partial R_P} \right) + \tau_P = 0. \end{cases} \tag{106}$$

In particular, the first equation takes the explicit form

$$\sigma(R_S^\top e_z e_z^\top R_P^\top R_Y^\top) = 0. \tag{107}$$

Such equations admit two solutions, namely

$$R_S R_Y R_P e_z = \pm e_z. \tag{108}$$

The left-hand side of the above relation represents the direction of the pendulum shaft as seen from the inertial reference system, therefore the interpretation of the above equation is that there exist two points of equilibrium, one corresponding to the pendulum pointing downward in the direction of gravity, and one parallel to gravity albeit pointing upward.

The first equation in (106) implies the latter two and from the second and third expressions of such system it follows that equilibrium requires zero holding torques.

5. Numerical simulations

In order to be able to perform numerical simulations on the devised mathematical model, it is necessary to put into effect a numerical scheme suitable to keep unaltered the structure of the involved variables, with special reference to the attitude-indicator matrices R_S, R_Y and R_P.

A large number of scientific problems are most naturally described by systems of first-order differential and algebraic equations. Numerical methods for solving initial value problems are extremely important, because analytic solutions exist only in very special cases (e.g., for linear equations, exact equations, non-exact equations with integrating factors, and equations that are homogeneous of degree 0). Any first-order initial value problem can be solved (or "integrated") numerically by discretizing the interval of integration into a number of sub-intervals, either with equally or non-equally distributed grid points. As the integration advances, the numerical solutions at the grid points are approximated.

In recent years, it has come to the attention of researchers in applied sciences and engineering how classical numerical methods, designed to solve initial value problems on $\mathbb{R}^n$ are unsuitable to solve differential equations formulated on differentiable manifolds. These differential equations compactly represent large systems of mixed non-linear differential/algebraic equations, where the algebraic sub-equations carry on mutual constraints among the variables.

Section 5.1 provides some details on numerical integration schemes suitable for the present endeavor. Section 5.2 summarizes the values of the parameters employed in the numerical simulations whose results are illustrated in Section 5.3. In particular, the present section displays results of simple numerical simulations that were carried out without a specific goal and a specific guidance algorithm, namely, regardless of a controller design that would be out of scope in the context of the present endeavor.

5.1. Numerical schemes to integrate the differential equations of the mathematical model

For numerical simulation purposes, it is convenient to cast the equations of motion, as derived in Sections 3 and 4, in the following form

$$\begin{cases} \dot{\Omega}_S = E_S, \ \dot{\Omega}_Y = E_Y, \ \dot{\Omega}_P = E_P, \\ \dot{R}_S = R_S \Omega_S, \ \dot{R}_Y = R_Y \Omega_Y, \ \dot{R}_P = R_P \Omega_P, \\ \dot{q} = r R_S \Omega_S R_S^\top e_z, \end{cases} \tag{109}$$

where we have defined

$$\begin{bmatrix} E_S \\ E_Y \\ E_P \end{bmatrix} := \mathbb{J}^{-1} \left\{ \begin{bmatrix} \mathrm{ad}^\star_{\Omega_S} \left(\frac{\partial \ell_c}{\partial \Omega_S} \right) - (R_S^\top e_z) \diamond \left.\frac{\partial \ell}{\partial \gamma}\right|_{v=r\Omega_S R_S^\top e_z} - r\,(\Omega_S R_S^\top e_z) \diamond \left.\frac{\partial \ell}{\partial v}\right|_{v=r\Omega_S \gamma} - k_S\,\Omega_S \\ \sigma_Y \left(R_Y^\top \frac{\partial \ell_c}{\partial R_Y} \right) + \tau_Y - k_Y\,\Omega_Y \\ \sigma_P \left(R_P^\top \frac{\partial \ell_c}{\partial R_P} \right) + \tau_P - k_P\,\Omega_P \end{bmatrix} - \dot{\mathbb{J}} \begin{bmatrix} \Omega_S \\ \Omega_Y \\ \Omega_P \end{bmatrix} \right\} \tag{110}$$

for convenience. The quantities $\Omega_S(0)$, $\Omega_Y(0)$, $\Omega_P(0)$, $R_S(0)$, $R_Y(0)$, $R_P(0)$ and $q(0)$ are supposed to be known from the initial conditions and the functions τ_Y and τ_P are supposed to be either fixed or calculated through a control algorithm. In the latter case, the input variables may be functions of the state variables, notably the attitude matrices and the position vector.

By solving the above seven Eqs. (109) numerically it is possible to determine the four functions of time R_S, q, R_Y and R_P that afford visualizing the behavior of the spherical robot both statically and dynamically. The first step to proceed on a numerical simulation is to time-discretize the seven variables, which are functions of time, by a sampling interval $T > 0$. The second step consists in writing discrete-time counterparts of the seven equations of motion in (109).

The first, second, third and seventh equations in (109) are based on vector spaces $\mathfrak{so}(3)$ and $\mathbb{R}^3$, therefore the related numerical iteration method may be chosen in the realm of standard numerical recipes such as Euler or Runge–Kutta. The fourth, fifth and sixth equations, on the other hand, are based on the curved space SO(3) and cannot be solved through standard recipes. It is rather necessary to invoke special methods as explained, e.g., in [33].

All in one, we used the following stepping rules

$$\begin{cases} \Omega_S \leftarrow \Omega_S + T\, E_S, \\ \Omega_Y \leftarrow \Omega_Y + T\, E_Y, \\ \Omega_P \leftarrow \Omega_P + T\, E_P, \\ q \leftarrow q + r\, T\, R_S\, \Omega_S\, R_S^{\top}\, e_z, \\ R_S \leftarrow R_S\, \mathrm{Exp}(T\, \Omega_S), \\ R_Y \leftarrow R_Y\, \mathrm{Exp}(T\, \Omega_Y), \\ R_P \leftarrow R_P\, \mathrm{Exp}(T\, \Omega_P), \end{cases} \tag{111}$$

to be repeated over a number $N > 0$ of iterations. (The total duration of a numerical simulation, in terms of proper robot time, is $N \cdot T$ seconds.) In the above relations, the symbol 'Exp' denotes matrix exponential. Depending on the computing platform/development language of choice, matrix exponential may be computed by some sort of approximation (see, e.g., the function 'expm' in MATLAB) or even by closed-form matrix-type polynomials [29].

5.2. Values of the parameters involved in the mathematical model of the spherical robot

The mathematical model of the studied spherical robot comprises a number of parameters that quantify its mechanical and geometrical characteristics. The weight and size of a spherical robot made by a thin spherical shell, a yoke, and a pendulum would depend on several factors, such as the materials used, the size of the spherical shell, the weight of the yoke and pendulum, and the intended purpose of the robot.

We shall assume that the robot is designed for general-purpose use. The size of the spherical shell depends on the desired range of motion and the size of the components that need to be housed inside. The weight of the yoke and pendulum would depend on the size of the spherical shell and the amount of weight needed to provide the desired level of stability and control. A heavier pendulum would provide greater stability but would also increase the weight of the robot, while a heavier yoke would increase forward rolling speed by momentum transfer.

We shall break down the set of parameters as follows (all parameters values are expressed in International System units):

- **Parameters of the spherical shell**. We shall consider a thin shell of radius $r = 0.3$ m. If we assume a very thin spherical shell, then a mass of around 1 kg for the shell alone could be plausible. However, it is important to note that a very thin shell may not be very durable or provide much protection to the internal components of the robot, so the specific design and intended use of the robot would need to be taken into consideration. Therefore, we shall take a value $m_S = 2$ kg, which corresponds roughly to a thickness of 5 mm and to the mass density of expanded polystyrene foam or certain types of low-density polyethylene. To what concerns the coefficient of friction for the shell, we deemed appropriate to choose the value $k_S = 0.08$ N m s/rad.
- **Parameters of the yoke**. The size and mass of the metal yoke would depend on the specific requirements and constraints of the robot design. A plausible design is that of a rectangular yoke with a width $b = 0.2$ m, a length $h = 0.5$ m, which could fit inside the spherical shell with enough clearance for the pendulum and other components. The yoke is assumed to be quite heavy, to allow for a reasonable speed of the robot. The single-rod masses are $m_b = 2$ kg and $m_h = 5$ kg. To what concerns the coefficient of friction, in this case we deemed appropriate to choose the value $k_Y = 0.02$ N m s/rad.
- **Parameters of the pendulum**: The length and mass of the pendulum would depend on the specific design requirements of the robot, such as its overall size and weight. If the pendulum is meant to serve as a stabilization mechanism for the robot, a longer and heavier pendulum would provide better stabilization. However, a longer pendulum would require more space inside the spherical shell, while a heavier pendulum would increase the overall weight of the robot. We selected a length $l = 0.2$ m and a mass $m_P = 1$ kg. To what concerns the coefficient of friction for the pendulum, we deemed appropriate to choose the value $k_P = 0.05$ N m s/rad.
- **Gravitational acceleration**. The value of the gravitational acceleration pulling on the robot depends on the location where it is meant to be deployed. Assuming that its location is on Earth's surface, we may assume a value $g = 9.81$ m/s^2. If the spherical robot is dispatched to another location such as the Moon or Mars, the gravitational acceleration acting on the robot would be different than on Earth. (On the Moon, the gravitational acceleration is much weaker than on Earth, approximately 1.62 m/s^2, which is about $\frac{1}{6}$th of Earth's gravitational acceleration. On Mars, the gravitational acceleration is also weaker than on Earth, but not as much as on the Moon, with a value of approximately 3.71 m/s^2.)

These values are sufficient to evaluate all the remaining constant parameters to be plug into the equations of motion.

Other values of interest for consistency check are the maximum torques provided by the electrical direct-current (DC) motors connected to the yoke and to the pendulum. The maximum torque of a DC motor is typically specified by the manufacturer and depends on factors such as the design of the motor, the winding characteristics as well as the operating voltage.

For a spherical robot like the one considered in the present research paper, a DC motor connected to the yoke with a maximum torque rating of around 0.5 to 2 N m could be sufficient for basic locomotion. However, for more demanding tasks, such as climbing inclines or dragging heavy payloads, a motor with a higher torque rating would be necessary.

A DC motor can be used to provide torque to a pendulum system in different ways, such as to provide an initial displacement, to control the amplitude of the oscillation, or to control the frequency of the oscillation. Assuming that the pendulum in the spherical robot is not intended to oscillate and is only used as a passive stabilizing mechanism, the use of a DC motor in this context may not be necessary. However, if a DC motor is used to control the position or orientation of the pendulum, its maximum torque would depend on the specific requirements of its application. In particular, if a motor is used to rotate the entire spherical robot, the maximum torque required would depend on the mass and moment of inertia of the entire system, as well as the desired angular acceleration and speed.

Since the two DC motors need to be mounted inside the robot's hull, their weight an location would change the overall mass distribution and hence the overall inertia tensors. The mass of a DC motor depends on various factors such as the motor size, power rating, construction materials, and manufacturing quality. For small DC motors, such as those used in hobbyist robotics or small-scale industrial applications, the mass can be in the range of a few tens to a few hundreds of grams. In control design, such extras may be taken into account by introducing additional terms in the equations representing errors and nuisances.

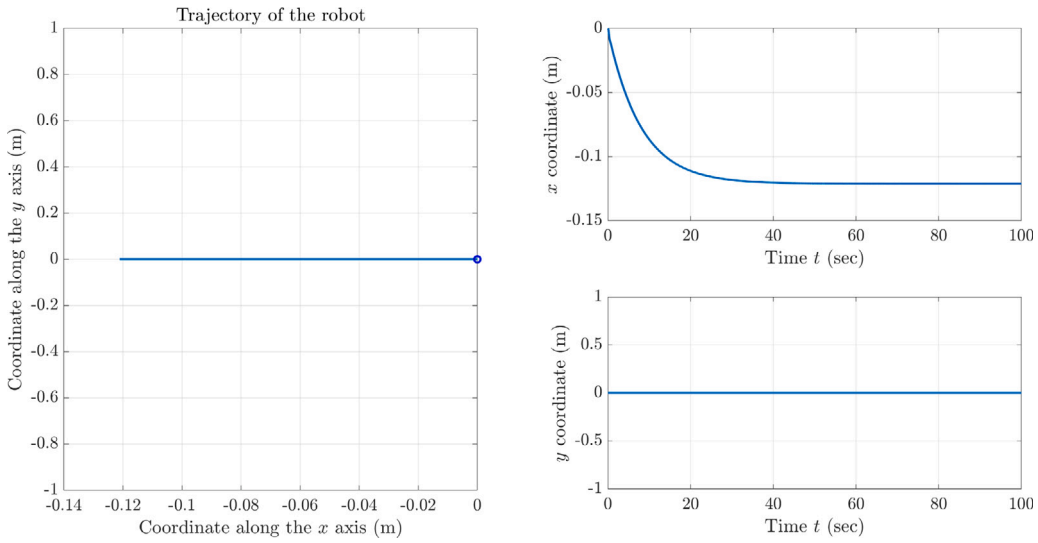

Fig. 2. Results of the experiment obtained with motors off, zero initial speeds, yoke initially at rest and pendulum shaft initially inclined: trajectory of the robot. The open circle denotes the starting point of the trajectory.

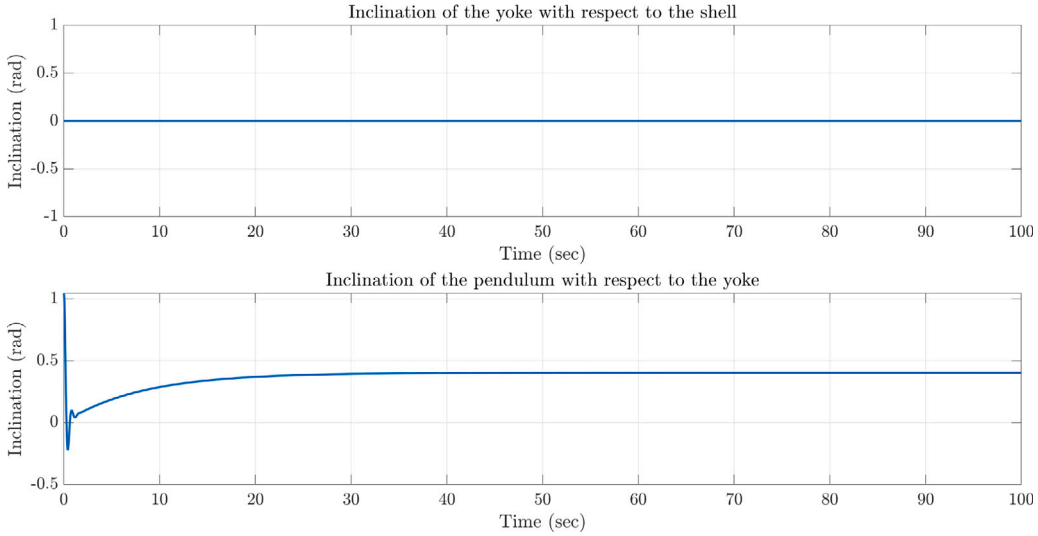

Fig. 3. Results of the experiment obtained with motors off, zero initial speeds, yoke initially at rest and pendulum shaft initially inclined: relative inclinations of the internal elements.

5.3. Results of numerical simulations

In the present section, we shall illustrate a few basic features of the devised model through three simulations whose results coincide to one's intuition. In all simulations, the sample interval was set as $T = 0.01$ s and the initial location of the robot was set as $q(0) = [0\ 0\ r]^\top$.

5.3.1. Simulation with zero torque, zero initial speeds and initially tilted pendulum shaft

In this simulation, the torques τ_P and τ_Y applied by the two DC motors to the pendulum shaft and to the yoke were set to zero. The initial angular velocities $\Omega_S(0)$, $\Omega_Y(0)$ and $\Omega_P(0)$ were set to zero as well. The initial attitude of the yoke $R_Y(0)$ and of the spherical shell $R_S(0)$ were set to the identity I_3, while the initial attitude $R_P(0)$ of the pendulum shaft was set to represent an initial condition where the shaft of the pendulum forms an angle of $\frac{\pi}{3}$ to the vertical axis $-e_z$.

Given this initial condition, the yoke will stay horizontal (with respect to the equatorial plane of the shell) while the pendulum will swing sideways, due to the force the gravity exerts on its center of mass, until coming to a rest due to energy dissipation caused by friction. As a reaction, the spherical robot will roll sideways. The trajectory of the center of mass of the robot – projected on the $z = 0$ plane – is illustrated in Fig. 2. The simulated dynamics results in no motion along the y axis and in a motion of a few centimeters along the x axis. No large sideways motion should be expected since the functions of the counter-weight pendulum are essentially stabilization and steering.

In this experiment, the number of numerical steps was set to $N = 10{,}000$, hence the total duration of the experiment is $N \cdot T = 100$ s. The inclination of the yoke and of the pendulum shaft are illustrated in Fig. 3. The yoke stays still, while the pendulum shaft oscillates slightly until coming to a rest (vertical) position. Due to the difference in inertia between the shell, the yoke and the pendulum, the swinging motion of the latter eventually results in a net motion of the robot along the x axis by way of momentum transfer.

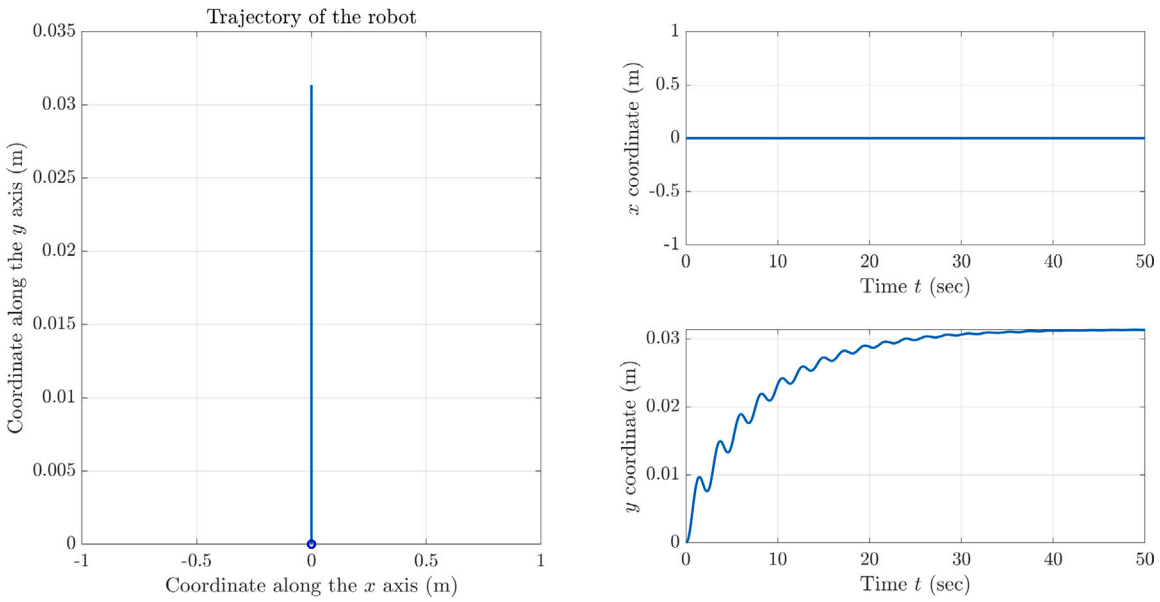

Fig. 4. Results of the experiment obtained with motors off, zero initial speeds, yoke initially inclined and pendulum shaft initially at rest: trajectory of the robot. The open circle denotes the starting point of the trajectory.

5.3.2. Simulation with zero torque, zero initial speeds and yoke frame initially tilted

In this simulation, again the mechanical torques τ_P and τ_Y applied by the two DC motors to the pendulum shaft and to the yoke frame were again set to zero and the initial angular velocities $\Omega_S(0)$, $\Omega_Y(0)$ and $\Omega_P(0)$ were set to zero as well. The initial attitude of the yoke $R_Y(0)$ was set to represent an initial condition where the frame of the yoke forms an angle of $\frac{\pi}{4}$ to the horizon, while the initial attitude of the pendulum $R_P(0)$ and of the spherical hull were set to the identity I_3, which corresponds to a pendulum initially at rest.

On the basis of such initial conditions, the shaft of the pendulum will not be swinging sideways throughout the whole simulation, while the yoke–pendulum system will swing forth and back, due to the force the gravity exerts on the pendulum, until coming to a rest due to energy dissipation caused by friction. As a reaction, the spherical robot will roll about the x axis on an oscillatory motion. The trajectory of the robot is illustrated in Fig. 4. The simulated dynamics results in no motion along the x axis and in a motion of a few centimeters along the y axis.

In this experiment, the number of numerical steps was set to $N = 5000$. The inclination of the yoke frame and of the pendulum shaft during the simulated experiment are illustrated in Fig. 5. The pendulum shaft stays still (in its own reference system), while the yoke frame oscillates until coming to a rest (horizontal) attitude. The swinging motion of the yoke–pendulum system results in a net motion of the robot along the y axis. Even though the motion appears steady, it is in fact slightly oscillatory.

5.3.3. Simulation with zero initial speeds, yoke and pendulum at rest, piece-wise constant torques

In the present last experiment, the yoke as well as the pendulum are initially at rest. From $t = 0$ to $t = 0.8$ s the motor connected to the yoke exerts a constant torque of magnitude 0.05 N and then the motor goes off. As a result, the robot is supposed to roll along a straight path parallel to the y axis of the inertial reference system $\mathcal{F}_{\mathrm{E}}$. From $t = 1.6$ s to $t = 1.8$ s, the motor connected to the pendulum is activated to exert a torque $\tau_P = -0.05\Sigma_P$ N and then goes off. From $t = 2.5$ s to $t = 3.0$ s, the DC motor connected to the yoke is activated again to exert a torque of -0.05 N. From $t = 3.4$ s to $t = 4.5$ s, the DC motor connected to the pendulum is activated for the last time to exert a torque of 0.05 N.

In this experiment, the number of numerical steps was set again to $N = 10{,}000$. The expectations on the motion of the robot are confirmed by the graphs shown in Fig. 6, which show a 'Γ-shaped' trajectory.

The Fig. 7 illustrates the inclination angles of the pendulum shaft and of the yoke frame as simulated numerically. The chosen overall time-frame of 100 s is sufficient to observe the whole dynamics. The net effect of the complex swinging motion of the yoke and of the pendulum along orthogonal axes is to cause locomotion, even though, in normal operations, locomotion is essentially obtained by swinging the yoke, while the pendulum is used to change direction and to stabilize the motion of the robot by lowering its center of mass.

6. Conclusion

Spherical robots have come a long way from their theoretical beginnings to becoming practical devices with a wide range of potential applications. Their development continues to be an area of research and innovation in the field of robotics.

In the present paper, we have recalled the formulation of non-conservative system dynamics through the non-holonomic Lagrange–d'Alembert principle for systems on manifolds and the generalized Euler–Poincaré (non-pure) form of the system equation on Lie groups. Such general formulation was applied to model a complex spherical robot actuated internally by a yoke frame and by a counter-weight pendulum.

Since the modeled robot was supposed to roll without slipping (on a horizontal surface), the locomotion of the robot is entirely due to its rolling motion, which casts a non-holonomic constraint on the associated phase space. The existence of such constraint affects the derivation of the equations of motion in a non-trivial way that was properly accounted for.

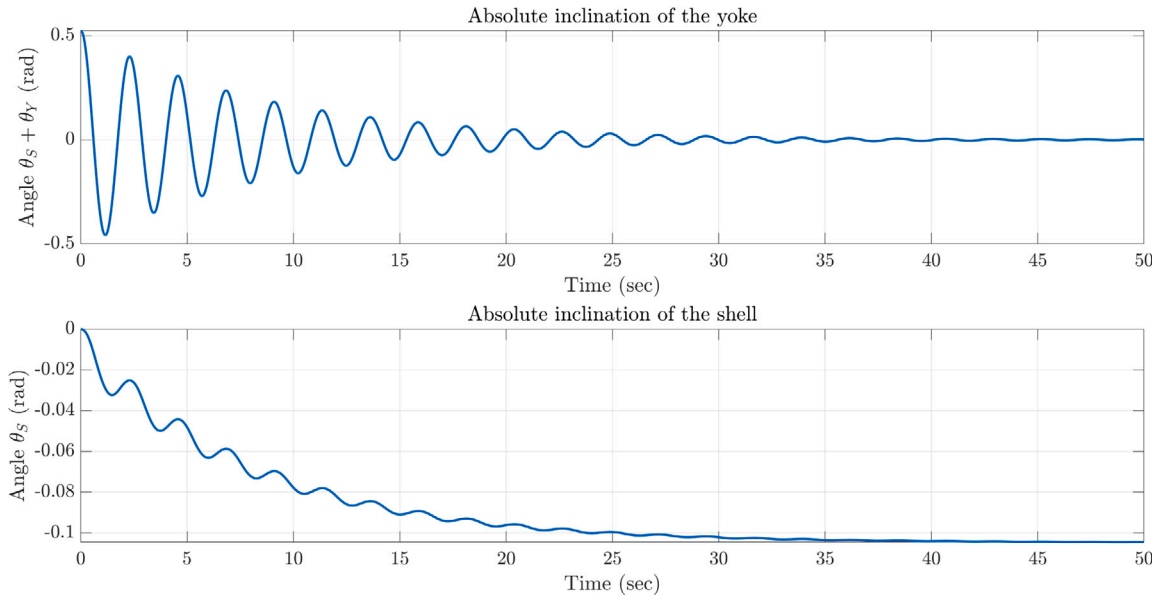

Fig. 5. Results of the experiment obtained with motors off, zero initial speeds, yoke initially inclined and pendulum shaft initially at rest: absolute inclinations (with respect to the inertial reference system).

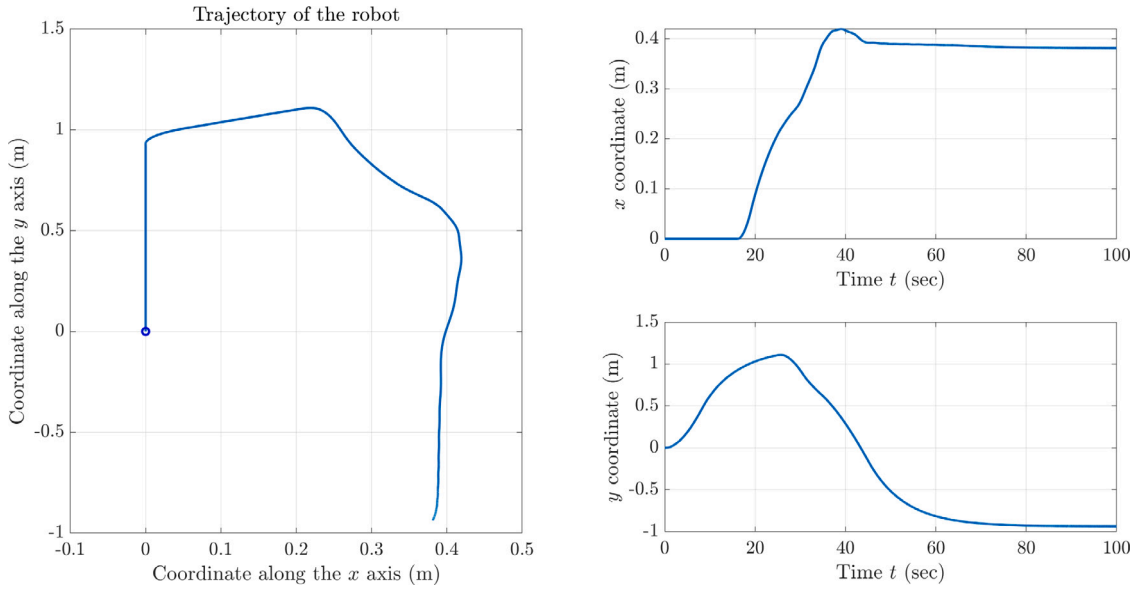

Fig. 6. Results of the experiment obtained with zero initial speeds, yoke and pendulum at rest, piece-wise constant torques: trajectory of the robot. The open circle denotes the starting point of the trajectory.

The outcome of such modeling endeavor is a set of equations, subdivided into Euler–Poincaré-type, reconstruction-type and advection type, which govern the evolution of the matrix–vector-type variables that describe the dynamics of the spherical robot. A distinguishing feature of the present endeavor is that no special coordinates were introduced to represent the position nor the attitude of the robot. Coordinates for such kinds of complex systems are non-universal and may prove quite difficult to get acquainted with [25,26].

In the present endeavor, we dealt with a problem of a complicated nonholonomic dynamic system modeling using Lie-group background. Contact between a moving body and a supporting surface was considered without a slipping possibility. Numerical experiments were carried out by a forward Euler method on manifold to integrate the equations of motion. A special integration rule, based on the exponential map, was invoked to integrate the reconstruction equations for the attitudinal variables of the three rotating components of the robot.

The potential of the recalled theoretical background appears to be large and paves the way to deeper examination about singular cases and their stability, existence of bifurcations (local and mainly global) and identification of trajectories with low stability.

The next step in the present endeavor will be to design a Lie-group based control algorithm to activate the actuators to either achieve orientation tracking or contact-point tracking. Such endeavor will require a specific design effort because of two main difficulties. The first one is that the

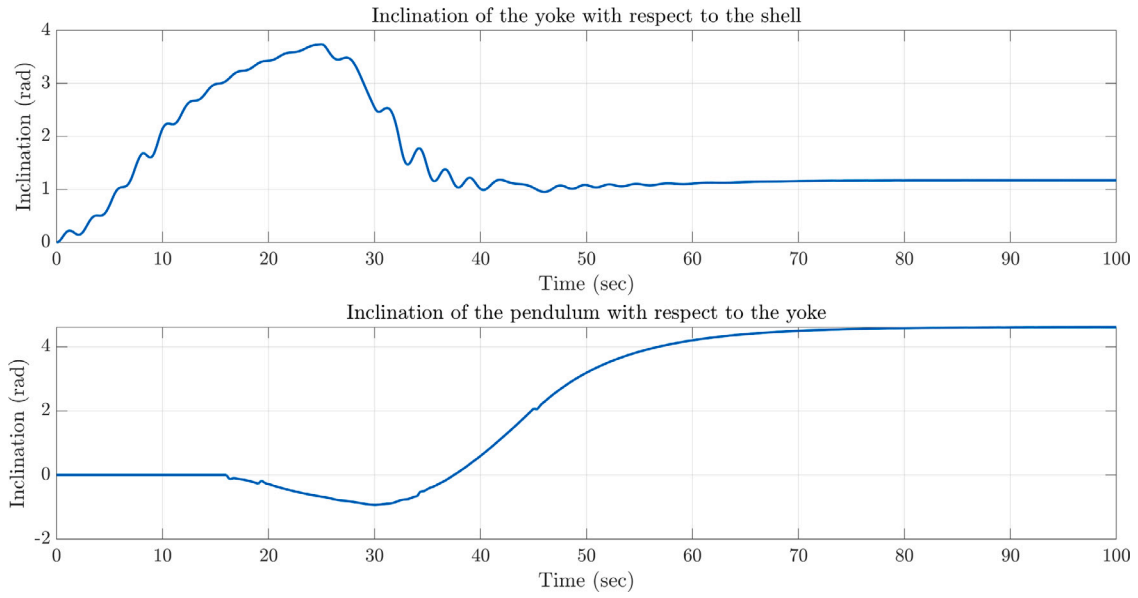

Fig. 7. Results of the experiment obtained with zero initial speeds, yoke and pendulum at rest, piece-wise constant torques: relative inclination of the internal elements.

studied robot model is underactuated, since the number of degrees of freedom exceeds the number of actuators, and the control torques do not influence the rotation speed of the shell directly but only indirectly through the oscillation of the yoke and the swinging of the pendulum. The second major difficulty is that the mathematical model devised in the present study is inherently non-linear, hence traditional linear control strategies do not apply.

CRediT authorship contribution statement

Simone Fiori: Conceptualization, Formal analysis, Investigation, Methodology, Software, Supervision, Validation, Visualization, Writing – original draft, Writing – review & editing.

Declaration of competing interest

The authors declare that they have no known competing financial interests or personal relationships that could have appeared to influence the work reported in this paper.

Data availability

No data was used for the research described in the article.

Acknowledgment

I would like to thank my former students, L. Severini and S. Sacchetti, who helped the present research by writing computer codes to simulate models of spherical robots known from the specialized literature.

Appendix A. Angular momentum due to the ground (non-slip) constraints

Let us define two generalized hull-related angular momenta

$$\Lambda_S := \frac{\partial \ell_c}{\partial \Omega_S}, \ \Lambda_S^{\mathrm{f}} := \left.\frac{\partial \ell}{\partial \Omega_S}\right|_{v=r\Omega_S\gamma}. \tag{112}$$

The angular momentum $\Lambda_S \in \mathfrak{so}(3)$ denotes the actual angular momentum of the robot expressed in the shell-fixed reference system, while the quantity $\Lambda_S^{\mathrm{f}} \in \mathfrak{so}(3)$ represents the 'free' angular momentum of the robot, namely, the rotational momentum as if all of a sudden the reaction of the ground that prevents the hull from slipping would vanish.

According to the Eq. (70), such angular momenta are related by the relationship

$$\Lambda_S = \Lambda_S^{\mathrm{f}} + r\left\{\gamma \diamond \left.\frac{\partial \ell}{\partial v}\right|_{v=r\Omega_S\gamma}\right\}. \tag{113}$$

The rightmost term in the above equation may hence be given an interesting interpretation as an angular momenta due to the reaction of the ground that prevents the contact point to the robot's hull to slip. As a matter of fact, it takes the form of a cross product between a generalized linear momentum $\left.\frac{\partial \ell}{\partial v}\right|_{v=r\Omega_S\gamma}$ and an arm $r\gamma$.

The discussed angular momentum $\Gamma := \Lambda_S - \Lambda_S^{\mathrm{f}}$ due to the non-slip reaction of the ground may be expressed explicitly as

$$\begin{aligned}\Gamma &= m_R r^2 \sigma(\gamma\gamma^\top \Omega_S) + m_P r \sigma(\gamma \bar{c}_P^\top R_P^\top R_Y^\top (\Omega_S + \Omega_Y + R_Y \Omega_P R_Y^\top)) \\ &= \sigma((m_R r^2 \gamma\gamma^\top + m_P r \sigma\gamma \bar{c}_P^\top R_P^\top R_Y^\top)\Omega_S) + \sigma(m_P r \sigma\gamma \bar{c}_P^\top R_P^\top R_Y^\top \Omega_Y) + \sigma(m_P r \sigma\gamma \bar{c}_P^\top R_P^\top \Omega_P R_Y).\end{aligned} \tag{114}$$

It appears as a combination of the angular velocities of each constituent of the robot. The movement of each part of the spherical robot, including the yoke and the pendulum, may cause the robot to skid if such action is not properly countered by the ground through a constrain reaction. The time-derivative $\dot{\Gamma}$ is nothing but a mechanical torque exerted by the ground reaction on the robot's hull.

Appendix B. Representation in yoke frame

It is possible to regard the reduced-constrained Lagrangian ℓ_c as a function of $\mathrm{Ad}_{R_Y}(\Omega_P)$, considered as a new independent variable, rather than as a function of the angular velocity matrix Ω_P, where the operator $\mathrm{Ad}_R : \mathfrak{so}(3) \to \mathfrak{so}(3)$, for every $R \in \mathrm{SO}(3)$, is defined as in (4).

The new Lagrangian function is defined in an implicit manner as

$$\bar{\ell}_c(\gamma, R_Y, R_P, \Omega_S, \Omega_Y, \mathrm{Ad}_{R_Y}(\Omega_P)) := \ell_c(\gamma, R_Y, R_P, \Omega_S, \Omega_Y, \Omega_P). \tag{115}$$

As a consequence, it is possible to express the fiber derivative $\frac{\partial \ell_c}{\partial \Omega_P}$ in terms of the fiber derivative $\frac{\partial \bar{\ell}_c}{\partial \mathrm{Ad}_{R_Y}(\Omega_P)}$. In fact, recalling that $\ell_c = \ell_c(\gamma, R_Y, R_P, \Omega_S, \Omega_Y, \Omega_P)$, we see that

$$\begin{aligned}\ell_c(\star, R_Y, \star, \star, \star, \Omega_P + \Delta\Omega_P) &= \bar{\ell}_c(\star, R_Y, \star, \star, \star, R_Y \Omega_P R_Y^\top + R_Y \Delta\Omega_P R_Y^\top) \\ &= \ell_c(\star, R_Y, \star, \star, \star, \Omega_P) + \left\langle \frac{\partial \bar{\ell}_c}{\partial \mathrm{Ad}_{R_Y}(\Omega_P)}, R_Y \Delta\Omega_P R_Y^\top \right\rangle^{\mathfrak{so}(3)} + \\ &\quad \mathcal{O}(\Delta\Omega_P) \\ &= \ell_c(\star, R_Y, \star, \star, \star, \Omega_P) + \left\langle R_Y^\top \frac{\partial \bar{\ell}_c}{\partial \mathrm{Ad}_{R_Y}(\Omega_P)} R_Y, \Delta\Omega_P \right\rangle^{\mathfrak{so}(3)} + \\ &\quad \mathcal{O}(\Delta\Omega_P).\end{aligned} \tag{116}$$

Therefore, we have that

$$\frac{\partial \ell_c}{\partial \Omega_P} = \sigma_P \left\{ R_Y^\top \frac{\partial \bar{\ell}_c}{\partial \mathrm{Ad}_{R_Y}(\Omega_P)} R_Y \right\} = \sigma_P \left\{ \mathrm{Ad}^\star_{R_Y} \left(\frac{\partial \bar{\ell}_c}{\partial \mathrm{Ad}_{R_Y}(\Omega_P)} \right) \right\}, \tag{117}$$

where $\mathrm{Ad}^\star$ denotes the dual of the operator Ad with respect to the metric $\langle \star, \star \rangle^{\mathfrak{so}(3)}$. We notice at this point that, while $\Omega_P \in \mathrm{span}\{\Sigma_P\} \subset \mathfrak{so}(3)$, it holds

$$\frac{\partial \bar{\ell}_c}{\partial \mathrm{Ad}_{R_Y}(\Omega_P)} \in \mathrm{span}\{\Sigma_P, \Sigma_C\} \subset \mathfrak{so}(3). \tag{118}$$

The explicit expression of the new reduced-constrained Lagrangian in the yoke reference system reads

$$\begin{aligned}\bar{\ell}_c(\gamma, R_Y, R_P, \Omega_S, \Omega_Y, \bar{\Omega}_P) &= \frac{1}{2} m_R r^2 \mathrm{tr}(\Omega_S \gamma\gamma^\top \Omega_S^\top) + \frac{1}{2} \mathrm{tr}(\Omega_S \hat{J}_R \Omega_S^\top) \\ &+ \frac{1}{2} \mathrm{tr}((\Omega_Y + \Omega_S) R_Y \hat{J}_Y R_Y^\top (\Omega_Y + \Omega_S)^\top) \\ &+ m_P r \gamma^\top \Omega_S^\top (\Omega_S + \Omega_Y + \bar{\Omega}_P) R_Y R_P \bar{c}_P \\ &+ \frac{1}{2} \mathrm{tr}\{(\Omega_S + \Omega_Y + \bar{\Omega}_P)(R_Y R_P \hat{J}_P R_P^\top R_Y^\top)(\Omega_S + \Omega_Y + \bar{\Omega}_P)^\top\} \\ &- m_P g \gamma^\top R_Y R_P \bar{c}_P + \text{constant},\end{aligned} \tag{119}$$

where the last addendum denotes again an unessential constant term.

In this representation, the linear combination of the matrices Ω_S, Ω_Y and $\mathrm{Ad}_{R_Y}(\Omega_P)$ is more involved than in the previous expressions. For this reason, it might be convenient to compute the fiber derivative $\frac{\partial \bar{\ell}_c}{\partial \mathrm{Ad}_{R_Y}(\Omega_P)}$.

The term $\mathrm{Ad}_{R_Y}(\Omega_P)$ is an element of the algebra $\mathfrak{so}(3)$ and belongs to a subspace spanned by the generators Σ_P and Σ_C. Let us introduce the operator $\bar{\sigma}_P$ that projects any 3×3 matrix into $\mathrm{span}\{\Sigma_P, \Sigma_C\}$. The fiber derivative of the Lagrangian (119) takes the form

$$\begin{aligned}\frac{\partial \bar{\ell}_c}{\partial \mathrm{Ad}_{R_Y(\Omega_P)}} &= \bar{\sigma}_P\{(R_Y R_P \hat{J}_P R_P^\top R_Y^\top + m_P r R_Y R_P \bar{c}_P \gamma^\top)\Omega_S + \\ &\qquad (R_Y R_P \hat{J}_P R_P^\top R_Y^\top)\Omega_Y + (R_Y R_P \hat{J}_P R_P^\top R_Y^\top)\mathrm{Ad}_{R_Y}(\Omega_P)\}.\end{aligned} \tag{120}$$

The terms involved in the fiber derivatives recast as

$$\begin{cases} \frac{\partial \ell_c}{\partial \Omega_S} = \sigma(M_{SS}\Omega_S + M_{SY}\Omega_Y + M_{SP}\bar{\Omega}_P), \\ \frac{\partial \ell_c}{\partial \Omega_Y} = \sigma_Y(M_{YS}\Omega_S + M_{YY}\Omega_Y + M_{YP}\bar{\Omega}_P), \\ \frac{\partial \bar{\ell}_c}{\partial \bar{\Omega}_P} = \bar{\sigma}_P(M_{PS}\Omega_S + M_{PY}\Omega_Y + M_{PP}\bar{\Omega}_P), \end{cases} \tag{121}$$

where we have defined matrices

$$\begin{cases} \bar{\Omega}_P := \mathrm{Ad}_{R_Y}(\Omega_P), \\ M_{SS} := m_R r^2 \gamma\gamma^\top + \hat{J}_S + R_Y \hat{J}_Y R_Y^\top + R_Y R_P \hat{J}_P R_P^\top R_Y^\top + m_P r(\gamma\xi^\top + \xi\gamma^\top), \\ M_{SY} := R_Y \hat{J}_Y R_Y^\top + R_Y R_P \hat{J}_P R_P^\top R_Y^\top + m_P r\gamma\xi^\top =: M_{YS}^\top, \\ M_{SP} := R_Y R_P \hat{J}_P R_P^\top R_Y^\top + m_P r\gamma\xi^\top =: M_{PS}^\top, \\ M_{YY} := R_Y \hat{J}_Y R_Y^\top + R_Y R_P \hat{J}_P R_P^\top R_Y^\top, \\ M_{YP} := R_Y R_P \hat{J}_P R_P^\top R_Y^\top =: M_{PY} =: M_{PP}, \end{cases} \tag{122}$$

which denote generalized, attitude-dependent, coefficients of inertia.

As a side note, the Lagrangian $\bar{\ell}_c$ is in fact a quadratic form in the variables Ω_S, Ω_Y and $\bar{\Omega}_P$, and the above matrices represent the coefficients of such quadratic form, that may be cast as

$$\bar{\ell}_c = \frac{1}{2}\mathrm{tr}\left\{ [\Omega_S^\top \quad \Omega_Y^\top \quad \bar{\Omega}_P^\top] \underbrace{\begin{bmatrix} M_{SS} & M_{SY} & M_{SP} \\ M_{YS} & M_{YY} & M_{YP} \\ M_{PS} & M_{PY} & M_{PP} \end{bmatrix}}_{=:S} \begin{bmatrix} \Omega_S \\ \Omega_Y \\ \bar{\Omega}_P \end{bmatrix} \right\} - m_P\, g\, \mathrm{tr}(\xi\gamma^\top), \tag{123}$$

where $S \in \mathbb{R}^{9\times 9}$ denotes a generalized inertia matrix and the placeholder ξ was defined in Section 2.6. Analogously, the fiber derivatives in (121) may be written compactly by introducing a generalized inertia operator $\mathbb{M} : (\mathfrak{so}(3))^3 \to (\mathfrak{so}(3))^3$ as

$$\begin{bmatrix} \frac{\partial \bar{\ell}_c}{\partial \Omega_S} \\ \frac{\partial \bar{\ell}_c}{\partial \Omega_Y} \\ \frac{\partial \bar{\ell}_c}{\partial \bar{\Omega}_P} \end{bmatrix} = \underbrace{\begin{bmatrix} \sigma(M_{SS}\bullet) & \sigma(M_{SY}\bullet) & \sigma(M_{SP}\bullet) \\ \sigma_Y(M_{YS}\bullet) & \sigma_Y(M_{YY}\bullet) & \sigma_Y(M_{YP}\bullet) \\ \bar{\sigma}_P(M_{PS}\bullet) & \bar{\sigma}_P(M_{PY}\bullet) & \bar{\sigma}_P(M_{PP}\bullet) \end{bmatrix}}_{=:\mathbb{M}} \begin{bmatrix} \Omega_S \\ \Omega_Y \\ \bar{\Omega}_P \end{bmatrix}. \tag{124}$$

From the expression of $\dot{\bar{\Omega}}_P$, it is desirable to infer the angular acceleration $\dot{\Omega}_P$ from which the value of the angular velocity Ω_P may be estimated numerically as well. To determine such relation, let us recall that $\bar{\Omega}_P = R_Y \Omega_P R_Y^\top$, therefore

$$\begin{aligned} \dot{\bar{\Omega}}_P &= \dot{R}_Y \Omega_P R_Y^\top + R_Y \dot{\Omega}_P R_Y^\top + R_Y \Omega_P R_Y^\top, \\ &= R_Y(\Omega_Y\Omega_P - \Omega_P\Omega_Y)R_Y^\top + R_Y \dot{\Omega}_P R_Y^\top \\ &= \mathrm{Ad}_{R_Y}(\mathrm{ad}_{\Omega_Y}(\Omega_P) + \dot{\Omega}_P). \end{aligned} \tag{125}$$

The inverse relationship that we were seeking therefore reads

$$\dot{\Omega}_P = \mathrm{Ad}^\star_{R_Y}(\dot{\bar{\Omega}}_P) + \mathrm{ad}^\star_{\Omega_Y}(\Omega_P). \tag{126}$$

To conclude this appendix, we notice that it is also necessary to express the quantity $\frac{\mathrm{d}}{\mathrm{d}t}\frac{\partial \bar{\ell}_c}{\partial \bar{\Omega}_P}$ as a function of $\frac{\mathrm{d}}{\mathrm{d}t}\mathrm{Ad}^\star_{R_Y}\left(\frac{\partial \bar{\ell}_c}{\partial \bar{\Omega}_P}\right)$ because the instantaneous value of the latter is known from the fifth equation of the system (85). From the given definitions, it holds that

$$\frac{\mathrm{d}}{\mathrm{d}t}\left(R_Y^\top \frac{\partial \bar{\ell}_c}{\partial \bar{\Omega}_P} R_Y\right) = \dot{R}_Y^\top \frac{\partial \bar{\ell}_c}{\partial \bar{\Omega}_P} R_Y + R_Y^\top \left(\frac{\mathrm{d}}{\mathrm{d}t}\frac{\partial \bar{\ell}_c}{\partial \bar{\Omega}_P}\right) R_Y + R_Y^\top \left(\frac{\partial \bar{\ell}_c}{\partial \bar{\Omega}_P}\right) \dot{R}_Y. \tag{127}$$

Henceforth,

$$\frac{\mathrm{d}}{\mathrm{d}t}\mathrm{Ad}^\star_{R_Y}\left(\frac{\partial \bar{\ell}_c}{\partial \bar{\Omega}_P}\right) = \mathrm{Ad}^\star_{R_Y}\left(\frac{\mathrm{d}}{\mathrm{d}t}\frac{\partial \bar{\ell}_c}{\partial \bar{\Omega}_P} + \mathrm{ad}^\star_{\Omega_Y}\left(\frac{\partial \bar{\ell}_c}{\partial \bar{\Omega}_P}\right)\right). \tag{128}$$

By inverting such expression, it turns out that

$$\frac{\mathrm{d}}{\mathrm{d}t}\frac{\partial \bar{\ell}_c}{\partial \bar{\Omega}_P} = \mathrm{Ad}_{R_Y}\left(\frac{\mathrm{d}}{\mathrm{d}t}\mathrm{Ad}^\star_{R_Y}\left(\frac{\partial \bar{\ell}_c}{\partial \bar{\Omega}_P}\right) + \mathrm{ad}_{\Omega_Y}\left(\frac{\partial \bar{\ell}_c}{\partial \bar{\Omega}_P}\right)\right). \tag{129}$$

As a result,

$$\frac{\mathrm{d}}{\mathrm{d}t}\frac{\partial \bar{\ell}_c}{\partial \bar{\Omega}_P} = \mathrm{Ad}_{R_Y}\left(\mathrm{ad}_{\Omega_Y}\left(\frac{\partial \bar{\ell}_c}{\partial \bar{\Omega}_P}\right) + \sigma_P\left(R_P^\top \frac{\partial \bar{\ell}_c}{\partial R_P}\right) + \tau_P\right), \tag{130}$$

which may be plugged into the third relation of (105) to complete the calculation.

Appendix C. Inverse of the generalized inertia operator $\mathbb{J}$

The projection operators involved in the expressions of the fiber derivatives are given explicitly as

$$\begin{cases} \sigma(M) = \frac{1}{2}\mathrm{tr}(\Sigma_Y^\top M)\Sigma_Y + \frac{1}{2}\mathrm{tr}(\Sigma_P^\top M)\Sigma_P + \frac{1}{2}\mathrm{tr}(\Sigma_C^\top M)\Sigma_C, \\ \sigma_Y(M) = \frac{1}{2}\mathrm{tr}(\Sigma_Y^\top M)\Sigma_Y, \\ \sigma_P(M) = \frac{1}{2}\mathrm{tr}(\Sigma_P^\top M)\Sigma_P \end{cases} \tag{131}$$

for any matrix $M \in \mathbb{R}^{3\times 3}$.

Let us consider the following equation

$$\begin{bmatrix} H \\ K \\ W \end{bmatrix} = \mathbb{J} \begin{bmatrix} X \\ Y \\ Z \end{bmatrix}, \tag{132}$$

with $H \in \mathfrak{so}(3)$, $K \in \mathrm{span}\{\Sigma_Y\}$ and $W \in \mathrm{span}\{\Sigma_P\}$ known matrices and $X \in \mathfrak{so}(3)$, $Y \in \mathrm{span}\{\Sigma_Y\}$ and $Z \in \mathrm{span}\{\Sigma_P\}$ unknown matrices to be determined by inversion. The solution to such equation provides a mean to compute the inverse $\mathbb{J}^{-1}$ of the generalized inertia operator.

The linear-algebra approach to such inversion problem hinges in writing down the three unknowns in components, as

$$\begin{cases} X = X_Y \Sigma_Y + X_P \Sigma_P + X_C \Sigma_C, \\ Y = Y_Y \Sigma_Y, \\ Z = Z_P \Sigma_P \end{cases} \tag{133}$$

where now the unknown are the five scalars $X_Y, X_P, X_C, Y_Y, Z_P \in \mathbb{R}$. Plugging such relations into the system (132) yields the three matrix identities

$$\begin{cases} H = \sigma(J_{SS}\Sigma_Y)X_Y + \sigma(J_{SS}\Sigma_P)X_P + \sigma(J_{SS}\Sigma_C)X_C \ + \sigma(J_{SY}\Sigma_Y)Y_Y + \sigma(J_{SP}\Sigma_P R_Y^\top)Z_P, \\ K = \sigma_Y(J_{YS}\Sigma_Y)X_Y + \sigma_Y(J_{YS}\Sigma_P)X_P + \sigma_Y(J_{YS}\Sigma_C)X_C \ + \sigma_Y(J_{YY}\Sigma_Y)Y_Y + \sigma_Y(J_{YP}\Sigma_P R_Y^\top)Z_P, \\ W = \sigma_P(J_{PS}\Sigma_Y R_Y)X_Y + \sigma_P(J_{PS}\Sigma_P R_Y)X_P + \sigma_P(J_{PS}\Sigma_C R_Y)X_C \ + \sigma_P(J_{PY}\Sigma_Y R_Y)Y_Y + \sigma_P(J_{PP}\Sigma_P)Z_P. \end{cases} \tag{134}$$

Even the three known matrices H, K, W may be expanded through the orthogonal basis $\{\Sigma_Y, \Sigma_P, \Sigma_C\}$ to be represented by five scalar coefficients $\frac{1}{2}\mathrm{tr}(H^\top \Sigma_Y)$, $\frac{1}{2}\mathrm{tr}(H^\top \Sigma_P)$, $\frac{1}{2}\mathrm{tr}(H^\top \Sigma_C)$, $\frac{1}{2}\mathrm{tr}(K^\top \Sigma_Y)$, $\frac{1}{2}\mathrm{tr}(W^\top \Sigma_P)$. The linear system to solve hence looks like

$$\begin{bmatrix} \mathrm{tr}(\Sigma_Y^\top J_{SS}\Sigma_Y) & \mathrm{tr}(\Sigma_P^\top J_{SS}\Sigma_Y) & \mathrm{tr}(\Sigma_C^\top J_{SS}\Sigma_Y) & \mathrm{tr}(\Sigma_Y^\top J_{SY}^\top \Sigma_Y) & \mathrm{tr}(R_Y \Sigma_P^\top J_{SP}^\top \Sigma_Y) \\ \mathrm{tr}(\Sigma_Y^\top J_{SS}\Sigma_P) & \mathrm{tr}(\Sigma_P^\top J_{SS}\Sigma_P) & \mathrm{tr}(\Sigma_C^\top J_{SS}\Sigma_P) & \mathrm{tr}(\Sigma_Y^\top J_{SY}^\top \Sigma_P) & \mathrm{tr}(R_Y \Sigma_P^\top J_{SP}^\top \Sigma_P) \\ \mathrm{tr}(\Sigma_Y^\top J_{SS}\Sigma_C) & \mathrm{tr}(\Sigma_P^\top J_{SS}\Sigma_C) & \mathrm{tr}(\Sigma_C^\top J_{SS}\Sigma_C) & \mathrm{tr}(\Sigma_Y^\top J_{SY}^\top \Sigma_C) & \mathrm{tr}(R_Y \Sigma_P^\top J_{SP}^\top \Sigma_C) \\ \mathrm{tr}(\Sigma_Y^\top J_{YS}^\top \Sigma_Y) & \mathrm{tr}(\Sigma_P^\top J_{YS}^\top \Sigma_Y) & \mathrm{tr}(\Sigma_C^\top J_{YS}^\top \Sigma_Y) & \mathrm{tr}(\Sigma_Y^\top J_{YY} \Sigma_Y) & \mathrm{tr}(R_Y \Sigma_P^\top J_{YP}^\top \Sigma_Y) \\ \mathrm{tr}(R_Y^\top \Sigma_Y^\top J_{PS}^\top \Sigma_P) & \mathrm{tr}(R_Y^\top \Sigma_P^\top J_{PS}^\top \Sigma_P) & \mathrm{tr}(R_Y^\top \Sigma_C^\top J_{PS}^\top \Sigma_P) & \mathrm{tr}(R_Y^\top \Sigma_Y^\top J_{PY}^\top \Sigma_P) & \mathrm{tr}(\Sigma_P^\top J_{PP} \Sigma_P) \end{bmatrix} \begin{bmatrix} X_Y \\ X_P \\ X_C \\ Y_Y \\ Z_P \end{bmatrix} = \begin{bmatrix} \mathrm{tr}(H^\top \Sigma_Y) \\ \mathrm{tr}(H^\top \Sigma_P) \\ \mathrm{tr}(H^\top \Sigma_C) \\ \mathrm{tr}(K^\top \Sigma_Y) \\ \mathrm{tr}(W^\top \Sigma_P) \end{bmatrix}.$$

Once the coefficients X_Y, X_P, X_C, Y_Y, Z_P are recovered by the solution of the above linear system, the sought unknown are calculated by the relations (133).

References

[1] F. Zhang, Y. Yu, Q. Wang, X. Zeng, H. Niu, A terrain-adaptive robot prototype designed for bumpy-surface exploration, Mech. Mach. Theory 141 (2019) 213–225, http://dx.doi.org/10.1016/j.mechmachtheory.2019.07.008, URL https://www.sciencedirect.com/science/article/pii/S0094114X19300758.

[2] S. Pecolt, A. Błażejewski, T. Królikowski, P.Z. Trzebiatowski, B. Schulz, Autonomous control of a mobile robot to explore areas with difficult terrain, Procedia Comput. Sci. 192 (2021) 3467–3476, http://dx.doi.org/10.1016/j.procs.2021.09.120, URL https://www.sciencedirect.com/science/article/pii/S1877050921018597. Knowledge-Based and Intelligent Information & Engineering Systems: Proceedings of the 25th International Conference KES2021.

[3] A. Torres-Pardo, D. Pinto-Fernández, M. Garabini, F. Angelini, D. Rodriguez-Cianca, S. Massardi, J. Tornero, J.C. Moreno, D. Torricelli, Legged locomotion over irregular terrains: state of the art of human and robot performance, Bioinspiration Biomim. 17 (6) (2022) 061002, http://dx.doi.org/10.1088/1748-3190/ac92b3.

[4] H.V. Alizadeh, Spherical Mobile Robot. https://www.cim.mcgill.ca/~hva/Spherical_Robot/.

[5] R. Chase, A. Pandya, A review of active mechanical driving principles of spherical robots, Robotics 1 (1) (2012) 3–23, http://dx.doi.org/10.3390/robotics1010003, URL https://www.mdpi.com/2218-6581/1/1/3.

[6] M. Li, H. Sun, L. Ma, P. Gao, D. Huo, Z. Wang, P. Sun, Special spherical mobile robot for planetary surface exploration: A review, Int. J. Adv. Robot. Syst. 20 (2) (2023) 17298806231162207, http://dx.doi.org/10.1177/17298806231162207.

[7] Sphero Edu Project. https://edu.sphero.com/sphero/home.

[8] F. Arzberger, A. Bredenbeck, J. Zevering, D. Borrmann, A. Nüchter, Towards spherical robots for mobile mapping in human made environments, ISPRS Open J. Photogramm. Remote Sens. 1 (2021) 100004, http://dx.doi.org/10.1016/j.ophoto.2021.100004, URL https://www.sciencedirect.com/science/article/pii/S2667393221000041.

[9] A. Singhal, S. Modi, A. Gupta, L. Vachhani, O.A. Ghag, Pendulum actuated spherical robot: Dynamic modeling & analysis for wobble & precession, IFAC-PapersOnLine 55 (22) (2022) 67–72, http://dx.doi.org/10.1016/j.ifacol.2023.03.012, URL https://www.sciencedirect.com/science/article/pii/S2405896323002707. 22nd IFAC Symposium on Automatic Control in Aerospace ACA 2022.

[10] NASA-Developed Spherical Robots to the Rescue. https://www.nasa.gov/directorates/spacetech/spinoff/NASA_Developed_Spherical_Robots_to_the_Rescue.

[11] J. Hernández, J. Barrientos, J. del Cerro, A. Barrientos, D. Sanz, Moisture measurement in crops using spherical robots, Ind. Robot 40 (1) (2013) 59–66, http://dx.doi.org/10.1108/01439911311294255.

[12] S. Sabet, M. Poursina, P.E. Nikravesh, Control of spherical robots on uneven terrains, in: 2021 IEEE/RSJ International Conference on Intelligent Robots and Systems, IROS, 2021, pp. 8159–8165, http://dx.doi.org/10.1109/IROS51168.2021.9636543.

[13] K. Schröder, G. Garcia, R. Chacón, G. Montenegro, A. Marroquín, G. Farias, S. Dormido-Canto, E. Fabregas, Development and control of a real spherical robot, Sensors 23 (8) (2023) http://dx.doi.org/10.3390/s23083895, URL https://www.mdpi.com/1424-8220/23/8/3895.

[14] G. Montenegro, R. Chacón, E. Fabregas, G. Garcia, K. Schröder, A. Marroquín, S. Dormido-Canto, G. Farias, Modeling and control of a spherical robot in the CoppeliaSim simulator, Sensors 22 (16) (2022) http://dx.doi.org/10.3390/s22166020, URL https://www.mdpi.com/1424-8220/22/16/6020.

[15] J. Náprstek, C. Fischer, Limit trajectories in a non-holonomic system of a ball moving inside a spherical cavity, J. Vib. Eng. Technol. 8 (2020) 269–284, http://dx.doi.org/10.1007/s42417-019-00132-1.

[16] J. Náprstek, C. Fischer, Stable and unstable solutions in auto-parametric resonance zone of a non-holonomic system, Nonlinear Dynam. 99 (2020) 299–312, http://dx.doi.org/10.1007/s11071-019-04948-0.

[17] J. Náprstek, C. Fischer, Trajectories of a ball moving inside a spherical cavity using first integrals of the governing nonlinear system, Nonlinear Dynam. 106 (2021) 1591–1625.

[18] S.-M. Lee, H. Son, Multi-sensor integration and fusion for control of multi-DOF spherical motion platform, Mechatronics 77 (2021) 102593, http://dx.doi.org/10.1016/j.mechatronics.2021.102593.

[19] X. Chi, Q. Zhan, Design and modelling of an amphibious spherical robot attached with assistant fins, Appl. Sci. 11 (9) (2021) http://dx.doi.org/10.3390/app11093739.

[20] S. Moazami, S. Palanki, H. Zargarzadeh, Kinematics of Norma, a spherical robot, rolling over 3D terrains, in: 2019 American Control Conference, ACC, 2019, pp. 1330–1335, http://dx.doi.org/10.23919/ACC.2019.8815194.

[21] S. Asiri, F. Khademianzadeh, A. Monadjemi, P. Moallem, The design and development of a dynamic model of a low-power consumption, two-pendulum spherical robot, IEEE/ASME Trans. Mechatronics 24 (5) (2019) 2406–2415, http://dx.doi.org/10.1109/TMECH.2019.2934180.

[22] H. Ge, Z. Ying, Z. Chen, W. Zu, C. Liu, Y. Jin, Improved A* algorithm for path planning of spherical robot considering energy consumption, Sensors 23 (16) (2023) http://dx.doi.org/10.3390/s23167115.

[23] Z. Ling, J. Zhang, R. Weng, B. Cai, B. Li, S. Zhang, G. Xiao, A dynamic-model-based predictive controller for a novel pendulum-driven spherical robot, in: 2022 7th International Conference on Robotics and Automation Engineering, ICRAE, 2022, pp. 191–198, http://dx.doi.org/10.1109/ICRAE56463.2022.10056223.
[24] S. Fiori, Manifold calculus in system theory and control – fundamentals and first-order systems, Symmetry 13 (11) (2021) 2092, http://dx.doi.org/10.3390/sym13112092.
[25] Q. Jia, H. Sun, D. Liu, Analysis of actuation for a spherical robot, in: 2008 IEEE Conference on Robotics, Automation and Mechatronics, 2008, pp. 266–271, http://dx.doi.org/10.1109/RAMECH.2008.4681363.
[26] D. Liu, H. Sun, Q. Jia, Stabilization and path following of a spherical robot, in: 2008 IEEE Conference on Robotics, Automation and Mechatronics, 2008, pp. 676–682, http://dx.doi.org/10.1109/RAMECH.2008.4681358.
[27] D. Schneider, Non-holonomic Euler–Poincaré equations and stability in Chaplygin's sphere, Dyn. Syst. 17 (2) (2002) 87–130, http://dx.doi.org/10.1080/02681110110112852.
[28] F. Gay-Balmaz, H. Yoshimura, Dirac reduction for nonholonomic mechanical systems and semidirect products, Adv. Appl. Math. 63 (2015) 131–213, http://dx.doi.org/10.1016/j.aam.2014.10.004.
[29] S. Fiori, Model formulation over Lie groups and numerical methods to simulate the motion of gyrostats and quadrotors, Mathematics 7 (10) (2019) http://dx.doi.org/10.3390/math7100935, URL https://www.mdpi.com/2227-7390/7/10/935.
[30] J. Náprstek, C. Fischer, Appell-Gibbs approach in dynamics of non-holonomic systems, in: M. Reyhanoglu (Ed.), Nonlinear Systems, IntechOpen, Rijeka, 2018, http://dx.doi.org/10.5772/intechopen.76258, Ch. 1.
[31] S. Gajbhiye, R.N. Banavar, Geometric modeling and local controllability of a spherical mobile robot actuated by an internal pendulum, Internat. J. Robust Nonlinear Control 26 (11) (2016) 2436–2454, http://dx.doi.org/10.1002/rnc.3457.
[32] A. Jain, Robot and Multibody Dynamics, first ed., Springer New York, NY, 2011.
[33] S. Fiori, L. Del Rossi, M. Gigli, A. Saccuti, First order and second order learning algorithms on the special orthogonal group to compute the SVD of data matrices, Electronics 9 (2) (2020) http://dx.doi.org/10.3390/electronics9020334, URL https://www.mdpi.com/2079-9292/9/2/334.

Simone Fiori received the M.Eng. degree in Electronic Engineering from Marches Polytechnic University in 1999 and the Ph.D. degree in Electrical Engineering from the University of Bologna in 2002. He currently holds the position of Associate Professor at the Department of Information Engineering at Marches Polytechnic University and of Visiting Professor at Peng's Lab at the Keio University (Japan). His current research interests and teaching activity include modeling and simulation of complex aircrafts and spacecrafts, modeling, simulation and control of complex underwater vehicles, simulation and control of DC power converters, optimization on manifolds and Lie groups, statistics on smooth manifolds, non-linear oscillation theories on Lie groups and smooth manifolds, non-linear control on smooth manifolds and related numerical calculus techniques.